STUDY OF EARLY SIGNALING EVENTS IN T CELL ACTIVATION ENABLED THROUGH A MODULAR AND MULTI-TIME POINT MICROFLUIDIC DEVICE

A Thesis
Presented to
The Academic Faculty

by

Catherine-Aurelie RIVET

In Partial Fulfillment
of the Requirements for the Degree
Master of Science in BioEngineering

Georgia Institute of Technology
December 2008

STUDY OF EARLY SIGNALING EVENTS IN T CELL ACTIVATION ENABLED THROUGH A MODULAR AND MULTI-TIME POINT MICROFLUIDIC DEVICE

Approved by:

Dr. Melissa L. Kemp, Advisor
School of Biomedical Engineering
Georgia Institute of Technology

Dr. Hang Lu
School of Chemical and Biomolecular Engineering
Georgia Institute of Technology

Dr. Oliver Brand
School of Electrical and Computer Engineering
Georgia Institute of Technology

Date Approved: November 13, 2004

A mes parents, à Vincent,
Pour leur présence et leur soutien

ACKNOWLEDGEMENTS

I wish to thank Professor Melissa Kemp, my Thesis Advisor, for the support and guidance she gave me these last 18 months. Working in her lab was really rewarding, I would like especially to thank her for her presence and all the conversations we had. I could not have better advisor.

I also would like to thank Professor Hang Lu for her encouragement and all the advice she gave me. She was always there to talk about little or bigger problems, and it was really reassuring.

I would like to thank Professor Oliver Brand for serving on my committee. I really appreciated his advice and support, and the course I attended with Professor Brand taught me a lot and helped increasing my knowledge on microelectromechanical devices.

I would like to thank Alison Hirsch, for all these mornings or afternoons we were spending together to run experiments, all the discussions we had to try to figure out and solve our issues, all the other discussions not always related to research. It was a pleasure to work with you.

I am also thankful to all the other members of the Kemp and Lu lab. Shreya Shukla was my mentor when I arrived and I thank her for the patience she had to teach me how to perform all the biological assays. I also would like to thank Abby Hill, who has been very helpful in some big experiments. Thanks also to Linda Kippner and Nnenna Adimora, with who I spent very good moments talking about research, politics, cats, or making fun of the words I was inventing. I hope the Kemp dictionary will have a long life.

Finally I would like to thank my boyfriend, Vincent Friedel and my parents. Both were really far away, Vincent in Sweden and my parents in France, but they always took the time to support and cherish me.

TABLE OF CONTENTS

LIST OF TABLES

LIST OF FIGURES

SUMMARY

Binding of the antigen receptor on T cells initiates a rapid series of signaling events leading to an immune response. To fully understand T cell mediated immunity, underlying regulatory properties of the receptor network must be understood. Monitoring dynamic protein signaling events allows for network analysis. Unfortunately, dynamic data acquisition is often extremely time-consuming and expensive with conventional methods; the number of proteins monitored at the same time on the same sample is limited. Furthermore, with conventional, multi-well plate assays it is difficult to achieve adequate resolution at sub-minute timescales. Microfluidics is a capable alternative, providing uniformity in sample handling to reduce error between experiments and precision in timing, an important factor in monitoring phosphorylation events that occur within minutes of stimulation. We used a two-module microfluidic platform for simultaneous multi-time point stimulation and lysis of T cells to investigate early signaling events with a resolution down to 20 seconds using only small amounts of cells and reagents. The device did not elicit adverse cellular stress in Jurkat cells. The activation of 6 important proteins in the signaling cascade upon stimulation with a soluble form of α-CD3 in the device was quantified and compared under a variety of conditions. First, in comparison to manual pipetting, the microdevice exhibits significantly less error between experiments. Secondly, a comparison between Jurkat cells and primary T cells shows similar dynamic trends across the 6 proteins. Finally, we have used the device to compare properties of long-term vs short-term cultured primary T cells. As expected, older cells present a much weakened response to antigenic cues, as

measured with TCR response markers. This modular microdevice provides a flexible format for investigating cell signaling properties through the use of soluble cue stimuli.

CHAPTER 1

INTRODUCTION

Mis en forme : Retrait : Première ligne : 0,42 cm, Tabulations :Pas à 0,63 cm

1.1 Motivation

1.1.1 Importance of T Cell signaling

The human immune system is composed of a collection of different cell types, working together to protect our bodies from bacterial, parasitic, fungal or viral infections, and against the growth of tumors. The process starts with the recognition of an antigen, which is displayed on the surface of a cell. If the antigen is recognized as “non-self”, the immune system will induce a signaling cascade to kill the invader. The first step of this immune response is made by the innate immune system, macrophages or dendritic cells. If the innate system can not fight against the pathogen by itself, they will become antigen presenting cells and activate T cells, lymphocytes from the thymus. The presentation of the antigen generates an immunological synapse. The presentation must be long enough to enable the mounting of an immune response, but not too long, otherwise the T-cell will undergo apoptosis. T cell receptor (TCR) activation, in naïve T cells, drives their differentiation and expansion. In mature T cells, it will drive expansion and triggering of effector functions, such as cytokine synthesis or cytotoxicity. (Nel, 2002)

A defect in T cell signaling leads to a large number of diseases. Autoimmune diseases and lymphoproliferative diseases such as multiple sclerosis, rheumatoid arthritis, lupus, type 1 diabetes, autoimmune lymphoproliferative syndrome (ALPS), come from a disruption of the surveillance mechanism leading to the tolerance of T cells to self-antigens. These T cells with high affinity for self peptide MHC do not undergo programmed cell death and usually escape functional inactivation (anergy) or extrathymic deletion. Inappropriate activation of these auto-reactive T cells leads to destruction of tissues and very serious diseases. (Abbas 2002, Peggs *et al* 2008)

Some viruses, such as HIV, use T cells as their major site of infection and replication, and inhibit the ability of these cells to respond. (Jerome 2008)

1.1.2 Quantification of T cell properties for cancer

Immune-based therapies hold promise in cancer therapy by harnessing the body's natural defense mechanisms against tumors. One approach, adoptive T cell therapy, is currently being investigated for clinical feasibility. A challenge in translating adoptive T cell therapy into a useful tool for oncologists is the ability for tumor antigen-specific T cells to maintain functionality after expansion and once in the tumor environment. Before adoptive transfer, T cell clones are evaluated based upon their specificity or their functionality. Functionality is quantified by cytokine production or cytolytic activity. Although specificity is retained *in vivo*, exhaustion of T cells from culturing can result in anergy. In addition, tumor cells can also cause anergy *in vivo* by several inhibitory mechanisms. In order to continue clinical development of this immune-based therapy, there is a need for assays to establish the level of responsiveness *ex vivo* and *in vivo* to monitor the state of the transferred T cells.

Adoptive transfer therapy by transfusion of T lymphocytes into cancer patients has held promise for many years as a method of harnessing the power of the adaptive immune response for fighting tumors as "foreign" bodies. Landmark studies of adoptive transfer for treating metastatic melanoma (Yee *et al* 2000; Dudley *et al* 2002) have resulted in a number of additional applications to pursue clinical trials for metastatic melanoma as well as prostate cancer, non-Hodgkin's lymphoma, chronic lymphocytic leukemia, nasopharyngeal carcinoma, lung cancer, gastric cancer and renal cell carcinoma (June 2007). Many of the clinical trials currently underway utilize autologous T cells that are refined for their specificity or engineered to enhance their activity in vivo (Morgan *et al* 2006). The use of T cell clones for adoptive transfer allows for selective expansion for tumor antigens. The transfer of peptide-primed CD4+ clones has been found to enhance the anti-tumor immunoresponse (Ossendorp *et al* 1998), most likely due to their cytokine-mediated recruitment of other immune cells. Both CD8+ and CD4+ cells are susceptible to loss of effector function in vivo (Staveley-O'Carroll *et al* 1998; Zippelius *et al* 2004). Immune suppression due to tumors remains a significant obstacle in the development of

adoptive therapy treatment protocols (Matter *et al* 2007). Many mechanisms have been uncovered by which tumors evade recognition and tolerize T cells. Tolerization is induced in part by an imbalance between stimulatory co-receptors such as B7.1 and B7.2 and inhibitory co-receptors such as CTLA-4 (present on T_{regs}), B7-H1, and B7-H4 in the tumor microenvironment (Zou 2005).

Before an effective T cell transfer, T cell functionality must be evaluated prior to infusion into patients. The assessment of T cell responsiveness *ex vivo*, therefore, is the motivation for the work presented in this document.

1.1.3 Development of microfluidic devices

Microfluidics technology has emerged as an attractive method of sampling molecular processes due to the controlled environmental conditions and small analyte and/or reagent volumes needed. In addition to the traditional advantages associated with miniaturization, fluids at the microscale exhibits very interesting properties. In microscale environments, certain fluid phemomena such as laminar flow, surface tension dominating over body forces, fluidic resistance, diffusion or energy dissipation become more pronounced. (Bebee, 2002)

Laminar flow is deterministic and especially predictable. It means that for a specific time point, we are able to predict the position of a particle of fluid in a particular stream. Flow in microfluidics is characterized by low Reynolds Number ($\mathrm{Re} = \frac{\rho v L}{\mu}$, where ρ is the density of the fluid, v its velocity, L the characteristic length of the channel, and μ, the viscosity of the fluid), usually less than 10. In a context of laminar flow, streams in contact with each other will not mix except by passive diffusion, enabling an easy production of concentration gradients. If grooves or any other 3D microstructure are in the channels, the flow can become chaotic, thus enhancing mass transport (Whitesides 2006, Stroock 2002)

Micromachining of silicon or glass was the first fabrication process used to create microfluidic devices. Cheaper techniques as soft lithography of polymers, such as PDMS, appeared to enable the

expansion and the use of microfluidics for biological applications. Nowadays, a large number of biological assays exist on lab on a chip, such as DNA electrophoresis, enzyme assays, immunoassays (Groissman *et al* 2005, Paliwal *et al* 2007, King *et al* 2008, El-Ali *et al* 2007, Lu *et al* 2005, McClain *et al* 2005, *Sims et al* 2007, Lee *et al* 2006, Herr *et al* 2007)

The use of microfluidics for these assays, in addition to the small reagent consumption, provides uniformity in sample handling to reduce error between experiments. It is also particularly suitable for high-throughput analysis and automation (Thorsen *et al* 2002; Lee *et al* 2005).

Mis en forme : Retrait : Première ligne : 0,42 cm

1.2 Prior knowledge

1.2.1 Capturing cell responsiveness: State of Art

1.2.1.1 Conventional Techniques

The measure of the frequency of cytokine secretion with enzyme-linked immunospot (ELISPOT) is a general test to assess cell responsiveness (Dang *et al* 2007). Unfortunately, it can not be multiplexed and usually takes hours to perform. Furthermore, it is not able to correlate cytokine production in real time to protein activation dynamics.

Flow cytometry analysis of intracellular cytokine production after 4 hours of PMA (Phorbol 12-myristate 13-acetate) or antigen presenting cell exposure is also used to assess response by staining fixed, permeablized cells with anti-cytokine antibodies. Activation-induced cell death metrics (e.g. anti-caspase 8) can also be quantified in this manner. Advantages of flow cytometry are the small number of cells needed for analysis and the ability to identify population heterogeneity by the single-cell analysis. A disadvantage is the number of measurements that can be made in parallel is limited by instrumentation.

Recently, others have recognized the ability of using early activation events to evaluate T cell functionality. TCR downregulation occurs within minutes of T cell activation, and was used in one report to assess responsiveness efficiency of T cells by flow cytometry (Kohrt *et al* 2005). This

protocol, however, relied on 4 hours of stimulation before quantifying this early activation event. Moreover, the multi-laser cytometers are constrained for the number of proteins monitored on the same sample.

Cell lysis and biochemical detection of population averages remains the most widespread method of capturing intracellular signaling dynamics of protein pathways. To extract the necessary protein information the cell must be stimulated for a precise period of time and immediately lysed to extract intracellular proteins for downstream analysis. With conventional, multi-well plate assays it is difficult to achieve adequate resolution at sub-minute timescales.

1.2.1.2 Prior Microfluidic Devices

Many microdevices have been reported for culturing cells, stimulating with soluble factors, assaying gene expression and performing lysis (Whitesides 2006). The challenges of any on-chip assays are that the devices should minimize stress on the cells, should provide reproducible results, from experiment to experiment, should produce quantitative results comparable to or better than bench-top schemes, should be scalable to high throughput format, should minimize consumption of cells and reagents, and ideally provide the temporal resolution that the bench-top counterparts cannot achieve.

Cell lysis on chip has been performed by many different ways: chemically, mechanically, electrically or thermally. The chemical method is the most common. The main advantage of chemical lysis is that subsequent assays can be performed in buffers previously optimized for conventional biological studies (El-Ali *et al*, 2007), using surfactants that solubilize the lipid membranes. Carlo et al presented cell lysis on chip based on local hydroxide electro generation (Carlo *et al* 2005). To help with the dilution of the lysate in solution, some groups performed lysis of single cells in picoliters reactors (Irimia *et al* 2005, Wu *et al* 2004). Mechanical lysis of cells has been performed on a compact disk with the centrifugal forces (Kim *et al* 2004) or just by increasing shear forces on the surfaces of the cells. Electrical lysis is attractive because of its rapidity and lack of reagent. (Wang *et al*, 2006)

Previously El-Ali *et al* developed a device achieving cell stimulus and lysis on a microfluidic chip using segmented gas-liquid flow for rapid mixing (El-Ali 2005). This device was the first to demonstrate on-chip multiple step manipulation of cells with fast mixing, thereby allowing access to the early time-point detection of protein states. They looked at the dynamics of 3 proteins downstream TCR ligation, ERK, JNK and p38, and showed that a time delay of about 45 seconds appeared to exist between TCR activation and activation of these kinases. However, segmented gas-liquid flow induces a significant shear stress on the cells at the interface. Their range of activation was performed by changing the flow rate, and ranged from 10seconds to 160 seconds; however, it does not enable a parallel acquisition of data from multi time points, and the range of stimulation time is limited.

1.2.2 Background in TCR signaling

The T cell antigen receptor (TCR) is a recognition module on the T cell surface, composed of an αβ-heterodimer or a γδ-heterodimer, and a signal transducing module containing CD3ε, CD3δ, CD3γ and CD3ζ polypeptides. The recognition of peptides bound to the major histocompatibility complex (MHC) by the TCR leads to the transduction of signals across the plasma membrane, and to the induction of cellular responses involved in T-lymphocyte effector function (Davis et al, 1998; Weiss & Littman, 1994). An early and essential signaling event that occurs after TCR ligation is the phosphorylation of immunoreceptor tyrosine-based activation motifs (ITAMs), which are located in the cytoplasmic domains of the CD3 subunits, by the Src kinase Lck.

Lck phosphorylation results in the recruitment and activation of ζ-chain-associated protein kinase 70kDa (ZAP70), which binds to the phosphorylated ITAMs. Once bound, Zap70, in turn, phosphorylates LAT, a transmembrane protein with 10 sites of potential tyrosine phosphorylation. Phosphorylation of the C-terminal four sites allows binding and activation of a set of adapter molecules, including phospholipase Cγ (PLC-γ), growth factor receptor-bound protein 2 (Grb2), and Grb2-related adaptor downstream of Shc (GADS). The activation of the adopter molecules GADS and Grb2, linked to the adapter protein LAT, leads to the activation of Ras, and the mitogen activated

protein kinases (MAPKs), such as ERK. The recruitment of GADS to LAT facilitates also the phosphorylation of SLP76 and association with Vav. This leads to cytoskeletal arrangements at the immunological synapse for further signal propagation.

The binding and activation of PLC-γ and the adapter molecules GADS and Grb2 lead to the recruitment of additional molecules and/or the triggering of downstream signaling events. Activated PLC-γ cleaves phosphatidylinositol biphosphate (PIP2) to diacylglycerol (DAG) and inositol triphosphate (IP3). It leads to the release of Ca^{2+} from the endoplasmic reticulum. DAG activates protein kinase C (PKC), which leads to the nuclear translocation of the transcription factor NF-kB.

A new recent signaling pathway independent on LAT has been recently described. (Salvador *et al*, 2005). This alternative pathway involves activation of the kinase p38, which may be directly phosphorylated by ZAP-70. p38-dependent TCR signaling appears to favor a predominantly Th2-type response, characterized by synthesis of cytokines such as interleukin- 4 (IL-4), IL-5, IL-13 and, especially, IL-10.

Costimulatory receptors also plays a big role in initiating an immune response. CD28 is one of the most studied ones. In the absence of CD28 costimulation, TCR ligation induces a much weakened response that can lead to anergy. CTLA-4 (which has the same ligands as CD28), or PD-1 (programmed cell death receptor 1) are inhibitory co-receptors, inducing the activation of phosphatases such as PP2A (protein phosphatase 2A), Shp-1 or Shp-2, that dephosphorylate molecules within the TCR pathway. (Song *et al* 2008)

Kemp et al demonstrated the suitability of studying T cell receptor signaling downstream of the receptor by sampling across the entire kinase network, by generating a dataset of 1100 measurements to represent signaling and response of TCR activation by measuring the dynamics of activation under different altered peptide ligand stimulation conditions. Through time-dependent data acquisition, the quantitative propagation of varied ligand avidity from altered peptide ligands was correlated to the magnitude of cytokine response by IL-2 production with a partial least squares regression model. This

model quantitatively established the combined contributions of each kinase cascade to IL-2 as shown by experimentally verified predictions of Erk and Akt inhibition.

1.2.3 Senescence in T-Cell activity

Adoptive transfer therapy relies on large quantities of T cells that maintain effector function. Because the adoptive transfer of senescent cells will result in suboptimal outcomes (or completely failure to curb tumor growth), a standardized method that can quantitatively evaluate the sensitivity of T cells to antigenic cues will improve the consistency of immune-based therapies in cancer treatment.

Senescence designates the dysregulation and dysfunction of cellular processes associated with age. For immune cells, it is often associated with a weakened response to antigenic cues, leading to a complete lack of response. This deterioration of immune response is thought to be linked in the elderly with a higher susceptibility to have cancer, autoimmune diseases or infectious diseases (e.g. pneumonia, influenza, bronchitis) (Pawalec *et al*, 2000).

Senescence is also observed in cultured cells. In 1961, for the first time, Hayflick and Moorehead reported that cultured human fibroblasts have a limited lifespan. All somatic cells undergo a finite and predictable number of cell division before reaching an irreversible state of growth arrest. This Hayflick limit is inherent to the cell type. (Hayflick 1985)

Pawalec *et al* (2000) have showed that T cell clones, after a certain number of passages, have a decreased ability to undergo autocrine clonal expansion and a decreased production of IL-2. They showed some alterations in surface molecules, like the co-stimulatory CD28, which could explain their altered responsiveness to activation signals. Furthermore, old cells are more susceptible to undergo apoptosis instead of tolerance or response, after stimulation because the levels of anti-apoptotic protein bcl-2 decreases. More recently, Mazzati *et al* (Aging Cell, 2007) investigated which genes and signaling pathways were differentially expressed in immunosenescence. Differences in expression of the transcriptional factor AP-1 and Fos, a part of the heterodimeric AP-1 transcription factor, involved

in cellular proliferation, differentiation and inflammation are found in senescent cells. They also show upregulation of proteins implicated in apoptosis, such as PTPN13, which has a role in FAS ligand mediated apoptosis, and lymphotoxin B, involved in tumor necrosis factor associated factor dependent caspase independent apoptosis. Using mass spectometry, the authors identified profilin-1, a ubiquitous protein associated with actin remodeling and cellular motility, as an unambiguously identified protein that gets overexpressed in senescent T cells (2007, Proteome Science). A decreased membrane fluidity and calcium influx and an altered regulation of the redox sensitive transcriptional factor NFκB, are also associated with senescence.

Mis en forme : Retrait : Première ligne : 0,42 cm

1.3 Outline of thesis

It is very important to be able to evaluate the responsiveness *ex vivo*-expanded T cells accurately for cancer therapy. Capturing the early dynamics of T cell activation of *ex vivo* expanded clones would improve upon current measures of T cell functionality. This measurement would be optimal for evaluating whether transferred T cells have retained their response to antigenic stimulation under culture conditions. The microfluidic format requires small sample and enables high-throughput experiments, in turn providing the much needed feedback on the quality of T cell therapy during cancer treatment.

A microfluidic system has been designed to capture T cell activation at many time points, especially immediately within minutes after the stimulation, on a small population of cells. To demonstrate feasibility of using minute amounts of samples from the microfluidic assay, protein yield and activities were determined by biochemical assays. In addition, we measured cell stress responses to validate that the microfluidic assays are not changing the biochemical properties of the cells non-specifically. The first set of assays was performed on an immortalized cell line to help optimizing experimental conditions, but also to establish a set of baseline parameters that cells from donors can be compared to. We used primary human T cells that are either anergic by senescence or capable of being activated to

show that protein activation from early time points capture distinguishing dynamics of T cell activation.

CHAPTER 2

A PARALLEL MULTI-TIME POINT MICROFLUIDIC DEVICE FOR CELL STIMULATION AND LYSIS

The study of signaling pathways requires the collection of data with a very good time resolution. One may be interested in protein activation, mRNA expression, but in all cases, a controlled stimulation time and fast lysis have to occur. Microfluidics is a very good tool to achieve this temporal resolution, as the laminar behavior of the fluid enables a precise control of residence time and the automated process provides uniformity in sample handling to reduce errors between experiments.

Mis en forme : Retrait : Première ligne : 1,06 cm

2.1 Microfluidic system with rapid mixing, controlled stimulation and lysis of cells: Design and Characterization

The design and characterization of the device was performed by Alison Hirsch in the School of Chemical and Biomolecular Engineering.

Previously El-Ali et al. developed a device achieving cell stimulus and lysis on a microfluidic chip using segmented gas-liquid flow for rapid mixing (2005). This device demonstrated fast mixing and early time-point detection of protein states. However, it did not enable a range of different incubation periods to understand the dynamics of multiple proteins upon stimulation. The device used in this thesis work was designed to complete 8 time points in parallel with controlled rapid mixing, precisely timed stimulation, and rapid lysis.

A two-module approach was used. Cell-containing media and stimulus solution enter in the first module by 2 separate inlets, with the flow driven by pressure with syringe pumps. They are mixed and split into 8 equal streams. The majority of the incubation time occurs in the tubing leading to module

2. On module 2, the reaction is quenched and cells are lysed by mixing with cold lysis buffer to extract intracellular components. The total amount of reagents used for these 8 time-point sample collection includes only 1.3 mL of cell suspension and lysis buffer, and 0.7 mL of stimulus.

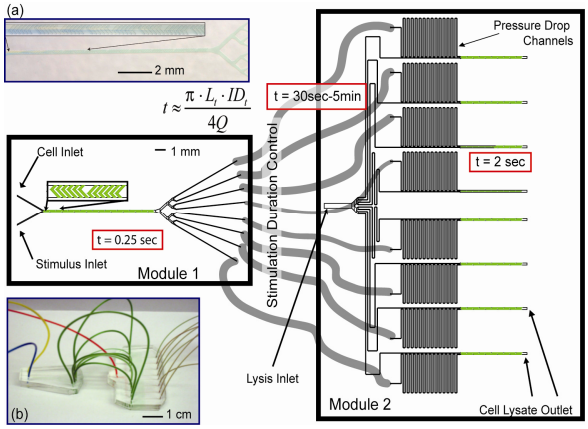

Fig. 1 A schematic of the devices showing inlets, tubing, pressure drop channels, and cell lysate outlets for sample collection. The respective residence times (t) in each unit are noted in red boxes on the figure, where the total time is essentially the time in the tubings, varying with length (L), inner diameter (ID), and volumetric flow rate (Q). Insets show (a) a close-up of Module 1 and (b) the whole device setup.

To ensure a precise definition of stimulation time, especially for the very early time points (e.g. 20 seconds), rapid mixing of cells with stimulus and lysis buffer is essential. If mixing takes a significant portion of the time compared to stimulation and lysis incubation, cells suspended in the initial medium will be immersed in the stimulant for different times, and the contact time cannot be precisely controlled.

The asymmetric herringbone mixer (HBM), developed by Stroock *et al* (2002), has been chosen as a fast, low-shear and flowrate-independent mixer. In order to design proper mixers for our application and determine an accurate starting time of incubation, Alison Hirsch developed computational fluid dynamics (CFD) models for different geometries and experimental flow conditions using COMSOL, a finite element solver for non-linear partial differential equations. Because the buffers, cell solutions, and stimulation solutions can have different fluid properties, the model was also used to probe the

effects of viscosity and density on mixing. Further confocal microscopy experiments were used to visualize the mixing of solutions with mismatched properties.

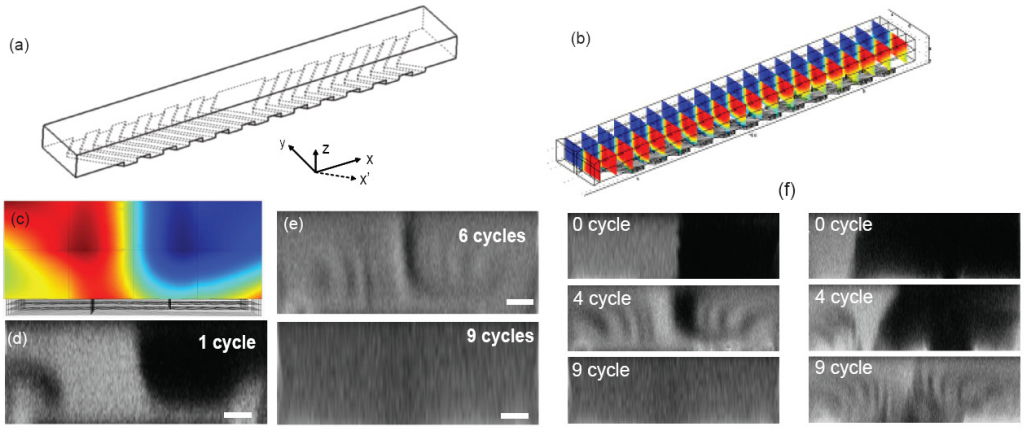

Fig. 2 a) One cycle schematic of the HBM. (b-d) Comparison of COMSOL model results with experiment. (b) perspective view of the mixing for 1 cycle of herringbone mixers. (c) y-z plane of the concentration profile color map from the model after 1 cycle. (d) y-z view of a confocal image of mixing after a single cycle with one inlet containing rhodamine dye. (e) y-z mixing profile after 6 and 9 cycles. The scale bar is 20 µm, twice the average diameter of a T-cell. f) Confocal images of the cross section at increasing mixing cycles of herringbones, for comparison of mixing of different viscosity solutions; left, equal viscosity, right, mismatched viscosity.

Experimental and computational results for mixing of solutions with the same viscosity, mimicking cell and stimulus mixing conditions, suggest that most cells would come into contact with the stimulus after 6 cycles. After 9 cycles, the solutions are completely mixed. In contrast, when solutions with mismatched viscosity and density are mixed (as in the case of mixing cell suspension with lysis buffer) with the same HBM the streamline profiles and extent of mixing are qualitatively different. In this case, the mixing is slower and therefore less efficient. However, this effect occurs only at viscosity ratio above that of our experimental conditions and therefore the HBM is adequate for fast mixing of cells and stimulus in Module 1, and of cells and lysis buffer in Module 2.

With the channel dimensions and fluid flow rates of the optimized setup, the staggered herringbone array achieves full mixing of reagents with minimal shear in less than 0.2 seconds on the stimulation chip , and <0.9 seconds on the lysis chip. These times are less than 5 percent of the ~23-second

stimulation time, which was the shortest stimulation time in our experiments. Hence the mixing time does not significantly affect the time point data.

After mixing, the fluid is split into 8 streams on Module 1, each stream accomplishing a different time point by using interchangeable tubing of different lengths and diameters. To obtain an equal flow rates in each stream, long pressure drop channels were added to balance the channel resistance.

Mis en forme : Retrait : Première ligne : 1,06 cm

2.2. Microfluidic Device Fabrication Process

The two module device is fabricated using standard soft lithography technique (Xia, 1998). The modules are molded in poly(dimethyl-siloxane) (PDMS) (Dow Corning Sylgard 184, Essex-Brownwell Inc., McDonough, Ga) from a two layer SU-8 (Microchem Corp., Newton, MA) master. One layer of 50 µm thick SU-8 2050 was spun onto 100mm silicon wafer, baked, and exposed under UV light to define a negative image of the channel system in the resist. After baking to crosslink the exposed resist, another layer of 15 µm thick SU-8 2010 was spun ontop. This layer formed the staggered herringbone array. After the same bake and expose process, the wafers were developed using propylene glycol monomethyl ether acetate (Doe & Ingalls, Inc., Durham NC). The wafer was surface treated with tridecafluoro-1,1,2,2-tetrahydrooctyl-1-trichlorosilane (United Chemical Technologies, Inc, Bristol PA) for surface passivation. Then PDMS was molded on the SU-8 master for 2 h at 70 ^{o}C. The PDMS was peeled off the mold and individual devices were cut to size. Medical grade polyethylene (PE) tubing (Scientific Commodities, Lake Havasu City, AZ) of various lengths and inner diameters were used to for fluidic connections. Holes for fluidic connections were punched to a size determined by the outer diameter of the appropriate tubing (21, 18, and 19 gauge for PE-1, -2, and -3 respectively).

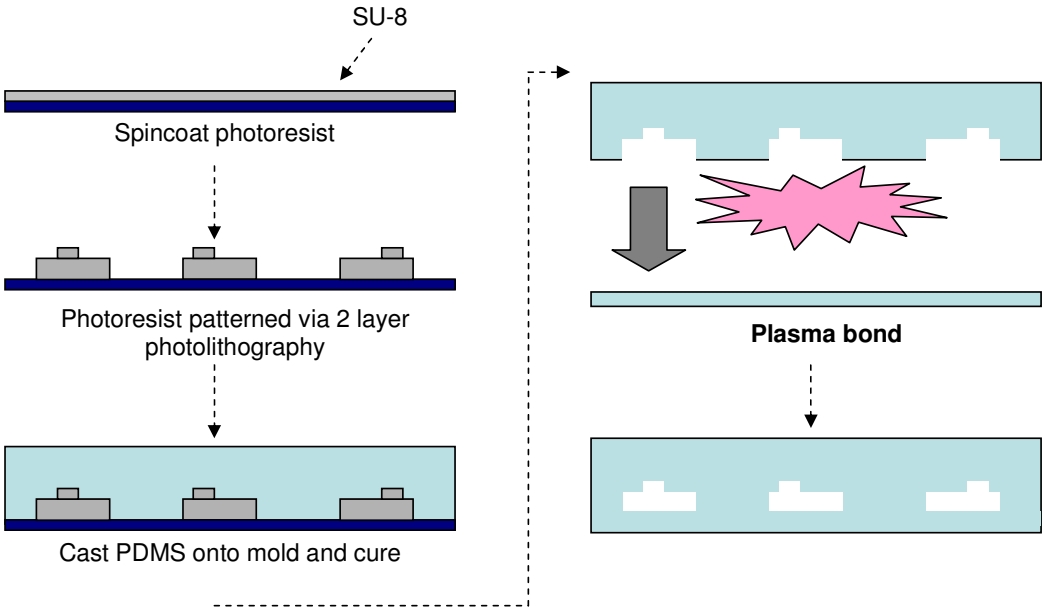

Fig 3. Adapted from Alison Hirsch. Standard Soft Lithography Process The photoresist is first spun onto a silicon wafer, patterned with a dark field mask, in a two layer process. After silanization, degassed PDMS is poured onto the silicon wafer and baked at 70°C for 3 hours. The molded PDMS is then plasma bonded to PDMS.

CHAPTER 3

PARALLEL ON-CHIP EXPERIMENTS FOR HIGH-THROUGHPUT MULTI-TIME POINT PROTEIN ACTIVATION ASSAYS

Understanding the dynamics of cell signaling networks is important to many biological applications, especially in complex disease phenotypes related to cancer, immune responses, development, and potential pharmacological interferences. Pathways involved in cell maintenance and apoptosis are studied extensively to understand cancer development (Janes *et al*, 2005, Reya *et al*, 2005). Focus on particular signal-transduction cascades and molecules has provided system-level insights into mechanism-based drug discovery (Sands, 2000, Gibbs, 2000)

Building a system-level computational model and gaining insights in to the complex signaling networks requires large data sets, presently a bottleneck in the process. For example, gene expression patterns or protein activity at various time points during stimulation with an external signal must be known; it usually takes many labs years to accumulate a large body of this type of data (Gaudet *et al,* 2005*,* Schoeberl *et al,* 2002, Kemp *et al,* 2007). Another challenge in signaling research is that many of these important protein activation events, such as phosphorylation, occur within minutes after stimulation (Kohrt *et al*, 2005, Kholodenko *et al,* 1999, Germain *et al,* 1999). Quantitative data not only at precise time points but early in the cells' response are necessary for accurate model generation.

3.1 Device operation and reliability

3.1.1 Cell distribution

3.1.1.1 Methods

For this study, we used Jurkat E6-1 human acute T-cell lymphoma from ATCC. Cells were cultured in RPMI 1640 medium with L-glutamine (Sigma-Aldrich) with 10 mM HEPES, 1mM Sodium Pyruvate, 1X MEM Nonessential Amino Acids, and 100 units/mL penicillin streptomycin (Cellgro),

Mis en forme : Retrait : Première ligne : 1,06 cm

Mis en forme : Police :Non Gras, Soulignement

supplemented with 10% certified heat inactivated fetal bovine serum (Sigma-Aldrich) at 37 °C in a humidified 5% CO2 incubator.

For the experiments, Jurkat E6-1 cells were resuspended in a phenol-red free RPMI 1640 medium (Sigma-Aldrich), supplemented with the previous reagents and 0.3 mg/ml of L-Glutamine (VWR). To prevent cell settling in the syringe, a 7wt % dextran powder was added to the prepared solution.

Before each experiment, each module was sterilized by flowing ethanol and water through it. Each microfluidic device was used only once.

After the cells were flowed through the microfluidic device, cells were counted with a hematocytometer.

3.1.1.2 Results and Discussion

Mis en forme : Police :Non Gras, Soulignement

Although fluid flow distribution was equal, cells were often observed to settle and aggregate. These aggregations in turn caused blockage on chips and together with settling, causing the cell distribution in the 8 collected samples to be non-uniform and unpredictable.

To resolve this issue, the media and stimulation solutions were supplemented with dextran to match the density of the cells (approx. 1.07 g/cm^3). In addition, dextran may also contribute to the suppression of unspecific adsorption of serum proteins in the medium which promotes cell adhesion to the walls. To determine the cell distribution after Module 1, regular medium was flown through the first inlet and cells at a known concentration, suspended in medium in the second inlet, both supplemented with dextran. The suspension in each outlet was collected and cells were counted with a hematocytometer to determine cell concentration. The average standard deviation of cell density in each stream was decreased by more than half compared to similar experiments without dextran. In addition, by taking the cells lost to settling in the syringes and devices into account, the resulting improvement by adding dextran is very significant.

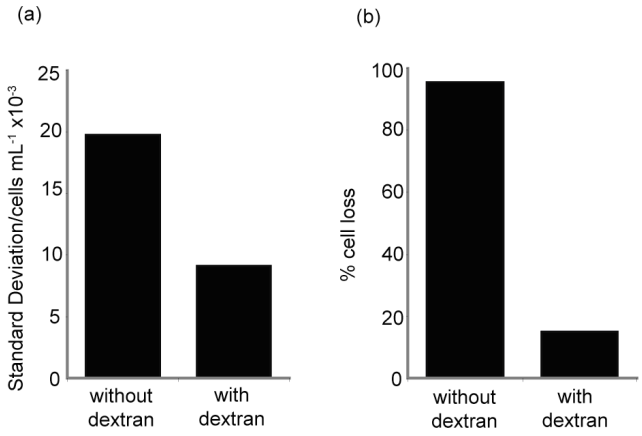

Fig. 4 The average standard deviation of cell concentration in each stream with and without dextran supplement in the solutions. The standard deviation between experiments is decreased by half with the addition of dextran and percent cell loss is markedly decreased.

Nevertheless, variability between cell concentrations per stream still exists. The addition of dextran only makes the uneven distribution predictable (Figure 5).

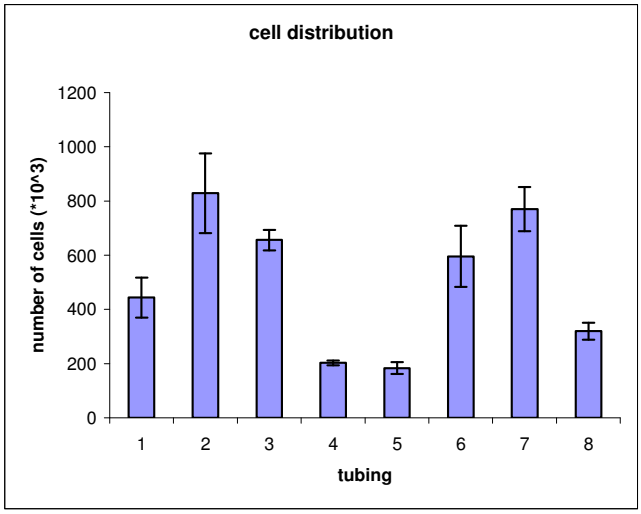

Fig. 5 Predictable but uneven split of cells within the first module after addition of dextran

In an attempt to improve the distribution, we changed the number of cycles of the herringbones (Figure 6). In fact, a simple channel splitting in 8 equal channels gives an even distribution of flow rates, but also of cells, so that we can confirm that the majority of cells follow the streamlines. The addition of herringbones changes the folding of the fluid and thus has an impact on the cell behaviour. None of our attempts to get a more even distribution was successful. Ten cycles of herringbones shifted the majority of the cells to the outlet 7. Eleven cycles was quite similar to 9 cycles, because it showed two peaks at outlet number 2 and 7, but the standard deviation between the outlets with the majority of the cells and the others was much more pronounced. Twelve cycles was similar to 10 cycles, and 13 cycles to 11 cycles. We could not try less than 9 herringbone cycles, which is the minimum number of cycles to make sure our reagents are mixed properly. It is very difficult to model the trajectories of particles in a channel with herringbone structures, without being limited by the computational power required. Attempts to use COMSOL, and its particle tracking tool to predict cell trajectories failed. The number of herringbone cycles seems to play a role in the cell distribution but we have not been able so far to understand how the cells behave in this structure. The distribution with 9 cycles being the more symmetric, we decided to use it for our further experiments.

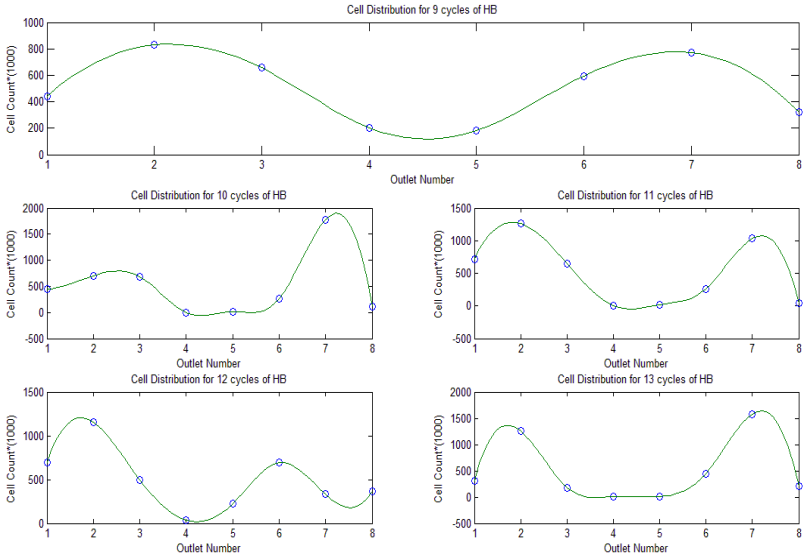

Fig. 6 Cell Distribution after the split in the first module for different number of herringbone cycles .

We tried then to see the impact of the flow rates on the cell distribution, reasoning that with a slower flow rate, the cells would follow more easily the streamlines. (Figure 7)

For this experiment, we used the 9 cycles HB device and modified the flow rate from 6.66 µL/min to 20 µL /min. This range was limited by the residence time in the mixing part compared to our smallest time points, and by the time we wanted the experiment to last. The maximum flow rate was chosen accordingly to the maximum shear stress the cell could bear before being activated.

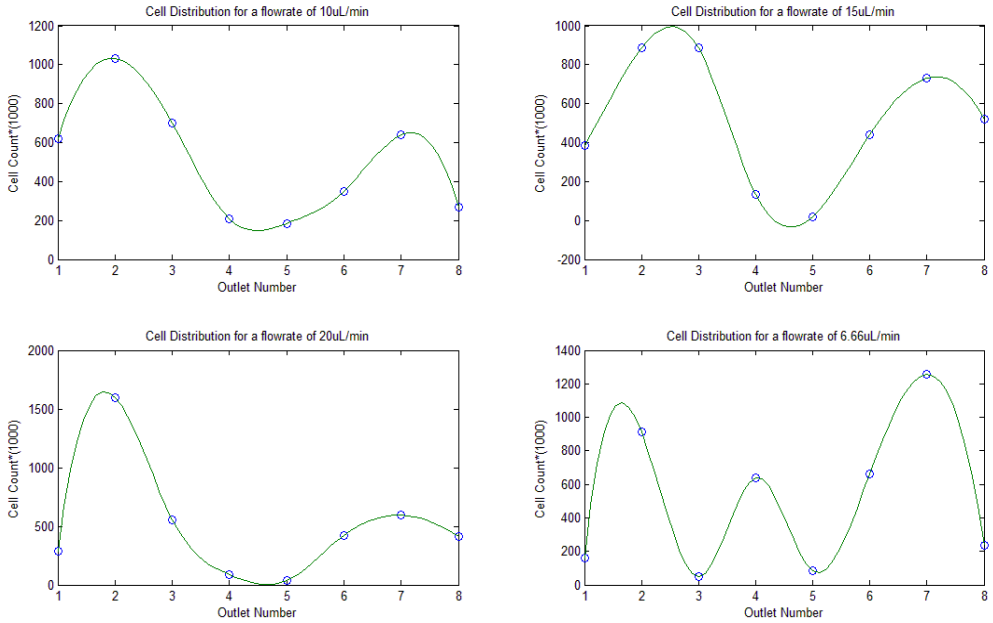

Fig. 7 Cell Distribution after the split in the first module for different flowrates ranging from 6.66 to 20 µL/min.

Changing the flow rate did not significantly enhance our distribution pattern. The slower flow rate gave us three peaks instead of 2 but the distribution was more unpredictable and the experiment much longer, which may induce errors if all the cells are left too long in the syringes (settling can occur even in the presence of dextran, cell death because of lack of nutrients and different lysis time). Faster flowrate increases shear stress on the cells and did not really improve the distribution, so the previous flow rate of 10 µL/min was kept for the subsequent experiments.

In another attempt to get a more even distribution, we decided to focus the cells after the HB mixers, by pinching the size of the channel before the splitting region. The original channel has a width of 100 µm and a length of 250 µm after the last cycle of HB before the split. In order not to clog the channel with the cells, whose diameter is about 10 µm, the width of the channel before the split has been decreased to 50 µm, for 250 µm and 500 µm in length. The pinching channel did not show significant improvement (Figure 8). The length after the last cycle of HB seemed to play a bigger role, but increasing it much further would have increased the incubation time, thus not enabling a good enough temporal resolution.

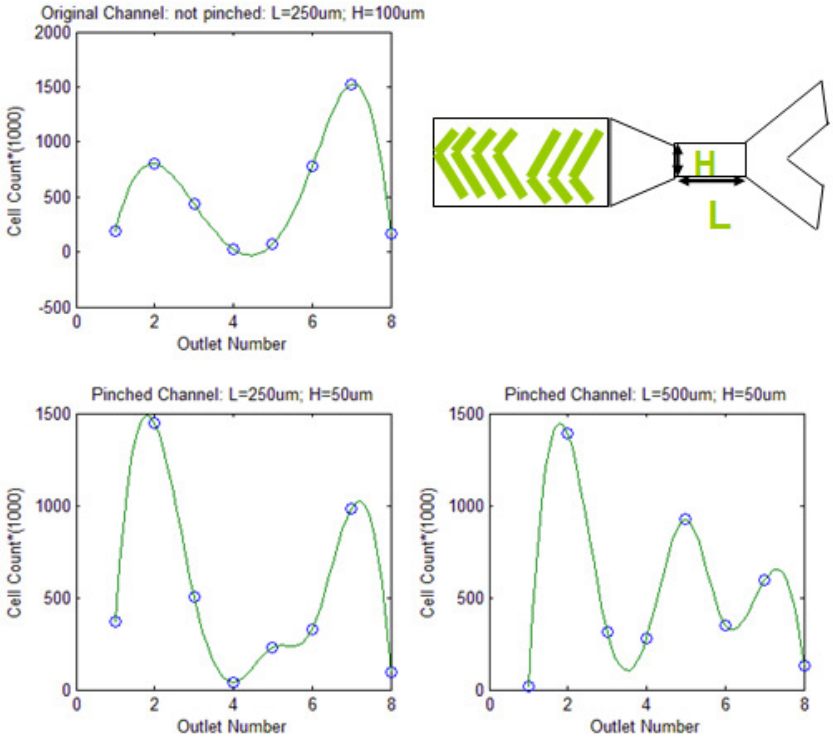

Fig. 8 Cell Distribution after the split in the first module for not pinched and pinched channel, for a 9 cycles HB mixer, and a flow rate of 10 µL/min. A simplified schematic of the pinching of the channel is shown on the top right of the picture.

From these experiments, we showed that cell distribution in herringbone structure is not trivial. Cells get focused in certain positions, and changing the flowrate or the the number of herringbone cycles has an effect on this distribution. Alison Hirsch is continuing this work, trying to model cell trajectories in simple herringbone structures.

3.1.2 Correlation between protein and cell distribution

Because the number of cells in all outlets are not the same, in order to quantify protein activation, we needed to be able to normalize for the cell numbers. Total protein concentration is a reasonable choice.

3.1.2.1 Methods

Mis en forme : Police :Non Gras, Soulignement

To obtain the total protein concentration from each outlet, both modules of the microfluidic device were used. In the first module, cells in a 7% dextran supplemented medium were mixed with the same medium. The tubings connecting both chips had the same length, as there is no need to obtain several time points. In the second chip, cells were mixed with a home-made cold lysis buffer. The lysis buffer used in these experiments was based on a 100% NP-40 solution (USBiological), supplemented with 1 M β-glycerophosphate (Calbiochem), 0.2 M sodium pyrophosphate (Alpha Aesar), 1 M sodium fluoride (EMD), 5 M Tris (Promega), 0.2 M sodium orthovanadate (Alfa Aesar), 5 M sodium chloride (Alfa Aesar), 100 mM benzamidine (Sigma), 500 mM EGTA (VWR), 5 mg/ml aprotinin (Sigma), 5 mg/ml leupeptin (VWR), 1 mg/ml pepsatin (Sigma), 1 mg/ml microcystin-LR (Sigma). Lysate solutions were collected at the outlets of the device, and centrifuged for 10 minutes at 14000rpm to remove the pellet. The total protein concentration was determined with a BCA assay kit (Pierce). In order not to interfere with the BCA assay kit, the medium used was phenol red and serum free.

3.1.2.2 Results and Discussion

Mis en forme : Police :Non Gras, Soulignement

The protein concentration obtained followed a distribution pattern very similar to the cells. The protein concentration could be correlated to the cell concentration from each outlet with a correlation coefficient of 0.85, as shown in Figure 9. To correlate cell and protein concentration from a single experiment, cells are first flowed through both devices, mixed two times with regular medium, and

collected. To acquire the lysates, the regular medium is switched with lysis buffer in the second module.

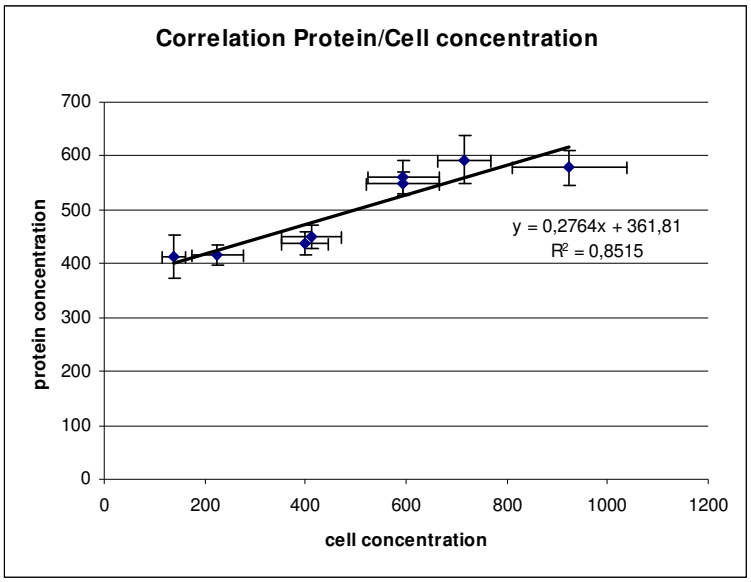

Fig. 9 Correlation between cell and protein concentration

Figure 9 shows that the total protein yield is linearly correlated to the number of cells in the sample, so that protein activity data can be easily normalized by the total protein in the sample. Using 5 to 8 million cells / mL of medium gave a sufficient protein yield, even for the outlets 4 and 5, usually devoid of the cells.

3.1.3 On-chip cell handling showing minimal stress on cells

For a microfluidic device to perform optimally for signal transduction applications, fluid forces must not impose adverse stresses on the cells within the chip. To validate that the cells flowing through the device were not subjected to undesirable shear stress due to fluid flow in narrow channels, undesirable mechanical forces produced by chaotic mixing, or lack of oxygen perfusion during the course of the experiment, the phosphorylation state of two MAPK proteins associated with stress response, p38 and JNK, were monitored.

3.1.3.1 Methods

Mis en forme : Police :Non Gras, Soulignement

Cells in dextran-supplemented medium, with no stimulatory reagents, were pumped through both modules of the microfluidic device. The lysates were compared to the results from cells lysed on bench top, also without any stimulation. For standard bench lysis, the addition was made by pipette addition of lysis buffer to microcentrifuge tubes containing the cells. The samples were incubated 30 minutes on ice, centrifuged at 14000 rpm for 10 minutes, and further protein analysis was performed with the supernatants.

The analysis of phosphorylation dynamics were performed with a Bio-Plex-200 instrument (Bio-Rad) using commercially available Luminex bead assays. The phospho-p38 and phospho-Jnk (Bio-Rad) measurements were performed following the manufacturer's protocol, after loading the same amount of protein in all the wells. To assess the success of the protocols, the lysates provided by the manufacturer were used as positive controls in the Luminex bead assay.

3.1.3.2 Results and Discussion

Mis en forme : Police :Non Gras, Soulignement

The levels of p38 and JNK activation for on-chip activation are constant over time and comparable to the results obtained on bench, demonstrating that the cells are neither adversely stressed by the conditions imposed by the flow through the microchannels, nor stressed by the time spent in the tubings (Figure 10). The lysates of Jurkat cells provided by the manufacturer gave similar values for the same amount of protein loaded.

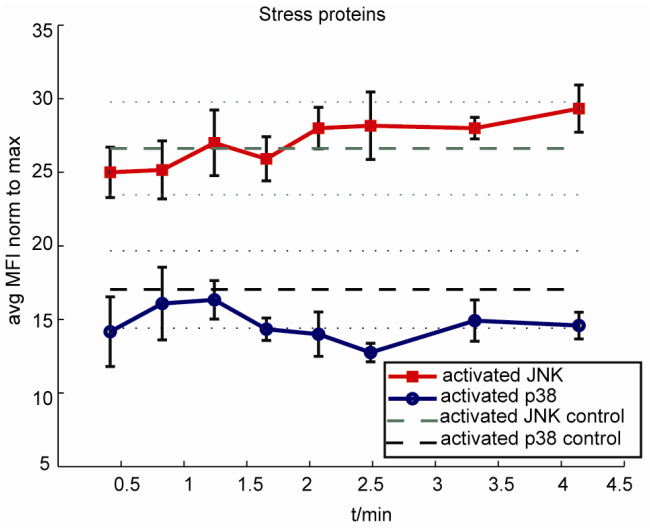

Fig. 10 Activated JNK and p38 concentrations in cells collected from the microfluidic devices compared to on bench controls, showing now signs of cellular stress induced by the device. For this experiment, samples were normalized to total cellular protein content. The experiments were run with three different devices and then the protein phosphorylation quantification was obtained with duplicates. Dashed lines represent the quantified values for phospho-p38 and phospho-JNK from control samples lysed on the bench. Dotted lines indicate standard deviation associated with the control values. Mean fluorescence intensity measurements for positive controls were comparable in magnitude to positive control lysates supplied by the manufacturer.

There was also no noticeable change in cell viability or morphology as observed by trypan blue exclusion after cells were subjected to flow through the device.

Mis en forme : Retrait : Première ligne : 1,06 cm

3.2 Multi-point TCR activation assay

3.2.1 Significance

The temporal regulation of protein activation during T cell receptor signaling involves multiple coordinated feedback loops, as reviewed by Germain *et al* (1999). Prior proteomic studies indicate widespread phosphorylation of signaling molecules occur within 5 minutes of T cell activation (Kim and White, 2006); thus, a method for consistent generation of sub-minute signaling events would be useful for extracting relationships between interconnected network components. To ensure that the microfluidic system is a reliable method of evaluating T cell activation, we characterized the

phosphorylation dynamics of representative signaling molecules downstream of the T cell receptor (Figure 10).

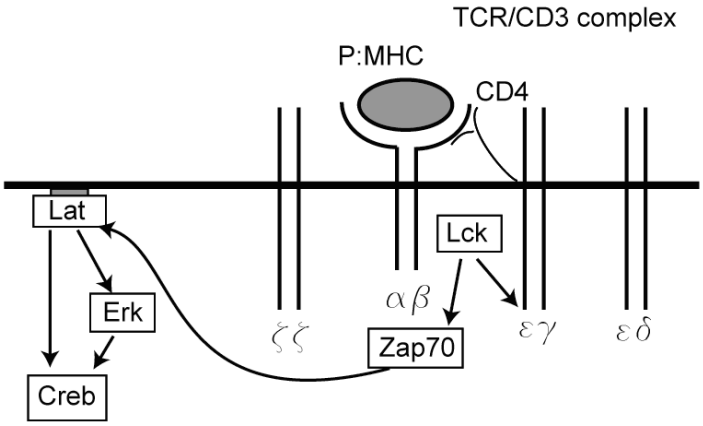

Fig. 11 Simplified pathway of TCR activation. After a peptide MHC has bound to the CD3/TCR complex , Lck phosphorylates the ITAM CD3, that recruits the tyrosine kinase ZAP70 to the complex. Zap70 phosphorylates then the adaptor protein LAT that activates the MAPK and the Ras pathway, the latter enabling the activation of Erk and Creb.

3.2.2 TCR activation in Jurkat Cells: Methods, Results and Discussion

Lysates were obtained from modules 1 and 2, with Jurkat cells treated with anti-human CD3, clone OKT3 (eBiosciences) at a final concentration of 2 µg/ml. To compare the efficiency of our micofluidic device, we have generated on bench standard stimulated lysates, as explained in the section 3.1.3.1. Comparisons between anti-CD3 (OKT3) stimulated Jurkat lysates generated by standard bench-top protocol and those generated by the device were made using the Beadlyte 7-plex human T-Cell receptor phosphoprotein signaling kit (Upstate). This kit quantifies phosphorylated ITAMs (CD3ε), ZAP-70, Lck, LAT, Erk, and CREB using the Luminex instrument as described by Khan *et al* (2007). Jurkat cells in a 7% dextran, phenol red and serum free medium were stimulated with the soluble form of anti-CD3 for the incubation times ranging approximately from 20 seconds to 4.5 minutes and then lysed with a cold lysis buffer containing phosphatase and protease inhibitors that prevent further biochemical events after lysis. The quantification of activated proteins downstream the TCR were

accomplished according to the manufacturer's protocol. Results for all data are presented as the average of three independent sets of experiments. To adjust for baseline changes between experiment days, mean fluorescence intensity for each protein assay across samples was normalized by the maximum value for the data.

Figure 11 shows the signaling dynamics for 6 proteins of interest for lysates generated by the microfluidic device and for lysates generated on bench.

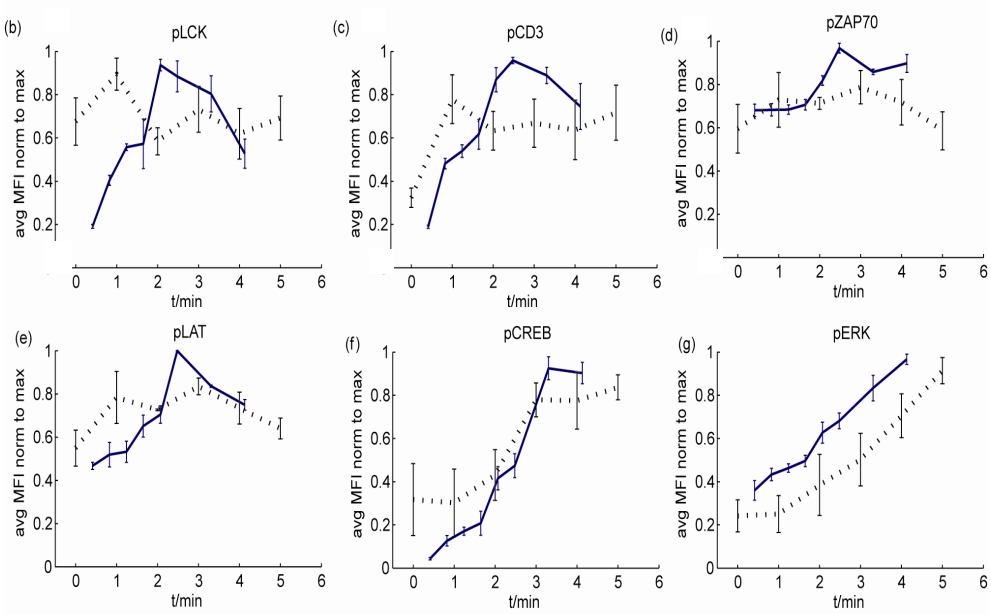

Fig. 12 For each of the selected protein, comparison of the dynamics obtained with the microfluidic device and those obtained by standard bench top protocol. The dynamics are very similar and the microfluidic device shows a better consistency in the results.

As illustrated in the simplified scheme of the TCR signaling cascade (Figure 10), the first proteins to be phosphorylated are CD3, Lck and Zap-70. Multiple signaling events occur before the downstream adaptor LAT, and the kinases Erk and CREB, are phosphorylated.

With the device, phosphorylation of CD3, Lck and Zap-70 starts after 2 minutes of stimulation and reaches its peak at 3 minutes. In contrast, the phosphorylation of Erk rises concurrently with the

downstream protein Creb over a longer period of 5 minutes. As expected, smaller variation occurs among samples across repeated experiments with the microfluidic device than with the manual stimulation and lysing, demonstrating a tight control over cell handling on-chip. The dynamic trends of activation are not dissimilar between the two experimental methods; however, an important feature emerges from the data. The uniformity of stimulatory exposure results in higher magnitudes of phosphorylation at early time points for all proteins measured. This is especially evident in the CD3 ITAM phosphorylation, possibly due to a flattened distribution of stimulated cells in the manual bench-top samples arising from the time lag of antibody:cell mixing. This feature highlights the necessity of consistent sample handling when quantifying cell population averages for signaling dynamics, especially when using small numbers of cells.

3.2.3 Application to primary T-Cells

Typically, 10^9-10^{11} cells are needed per patient for adoptive transfer therapy, a number that creates significant challenges in generating with uniform responsiveness and specificity. As a result, a plethora of different methods have emerged for expanding T cells *in vitro* – soluble anti-CD3/CD28 (Riddell and Greenberg 1990), magnetic antibody-coated beads (Kalamasz *et al* 2004), HLA tetramer-bound beads (Maus *et al* 2003), dendritic cells (Ho *et al* 2006), and engineered antigen presenting cells (Maus *et al* 2002; Oelke *et al* 2003). In some cancer applications, tumor antigen-specific T cells are being primed *in vivo*, then derived and expanded ex vivo (Dang *et al* 2007). The non-uniformity and lack of standardization of the T cell expansion process prevents reproducibility and hinders clinical translation (Barber *et al* 2006).

3.2.3.1 Methods

Mis en forme : Police :Non Gras, Soulignement

Upon IRB approval, 30 mL of fresh blood was collected from 3 healthy donors, in EDTA coated tubes. After dilution 1:1 in a 0.9% NaCl solution, 30mL of diluted blood is layered on top of 15mL of density gradient medium, Lymphoprep, without mixing both liquids. After centrifugation at 800g for 20 minutes, at 22°C, the peripheral blood mononuclear cells (PBMC) layer is removed with a 1mL pipette, leaving undisturbed the plasma layer (Figure 13).

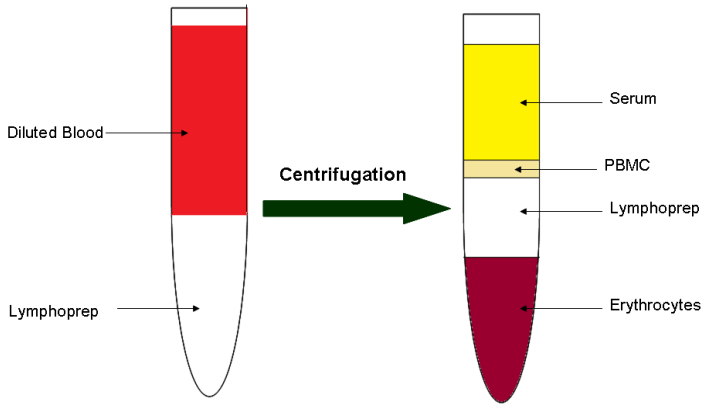

Fig. 13 The peripheral blood mononuclear cell layer is obtained by centrifugation of diluted blood with a gradient density medium, here lymphoprep.

To remove platelets, this PBMC layer is washed twice with PBS, 0.1% BSA at 250g, for 10 minutes. The cells are then counted and resuspended in isolation buffer (PBS, 2mM EDTA) at 10^8 cells/mL. A typical extraction process provides 40 to 70 millions of mononuclear cells. T cells are further extracted by depletion, using the T cell depletion kit from Invitrogen (Dynal Beads). After the extraction, the cells are washed and put in culture in flasks with 2 beads (anti-CD3, anti-CD28, expansion bead, Dynal Bead, Invitrogen) per cell, in regular medium at 10^6 cells/mL. After 2 days of expansion, the cells are passaged and the medium is supplemented with 50U/mL of recombinant IL-2 (Sigma). The cells are then cultured for 2 weeks without restimulation, being passaged every two days and resuspended at $0.5 \cdot 10^6$ cells/mL.

To ensure the cells were not subjected to any stress after bead removal, we monitored by flowcytometry the expression of phosphorylated ERK for several time points after bead removal (Figure 14). After bead removal, the cells were resuspended in IL-2 supplemented media, during the length of the experiment. The cells were fixed with a 2% paraformaldehyde solution, then permeabilized in a 90% methanol solution, before being frozen. The samples were then thawed and stained with a 100x rabbit-pERK antibody (eBiosciences) and a 500x RPE donkey anti-Rabbit secondary antibody was used for visualization purposes. After 2 hours, the cells have lost 20% of their

phosphorylated ERK. After 5 hours, only 60% of pERK is remaining. For all the following experiments, we have removed the beads at least 48 hours before the experiment to ensure no cross talk between the data obtained from the stimulation by our anti-CD3 antibody and the stimulation remaining effect of the expansion beads.

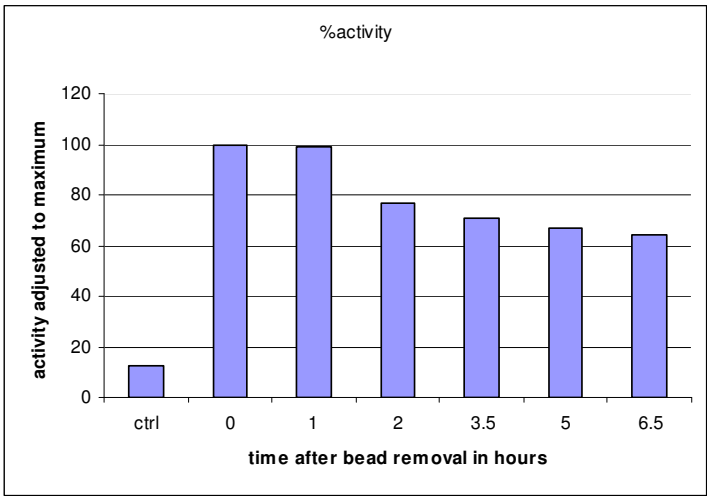

Fig. 14 The cells were fixed in 2% paraformaldehyde and stained for pERK. The activity of the activated ERK is normalized to the maximum activity at t=0 when the bead have just been removed.

For on-chip stimulation experiments, primary T-cells were resuspended in phenol-red and serum free medium, supplemented with 7% dextran. All the data were acquired with the same protocol than the one used for Jurkat Cells.

Mis en forme : Police :Non Gras, Soulignement

3.2.3.2 Results and Discussion

T cells from three healthy donors were extracted 6 days prior to the experiment.

Table 1 Characteristics of drawn blood from each donor.

* mean for the 8 first days of culture.

	Numbers of PBMC ($x10^6$)	Number of T cells ($x10^6$)	Division Rate (per day) *
Donor 1	67	40	1.45
Donor 2	38	24	1.74
Donor 3	66	20	1.65

At day 6, 8 million cells for each donor were harvested and flown through the microfluidic chip with stimulus and lysis buffer. Quantification of the 6 phosphorylated proteins for the 3 donors showed a clear trend among the donors despite the variations from patient to patient (Figure 15).

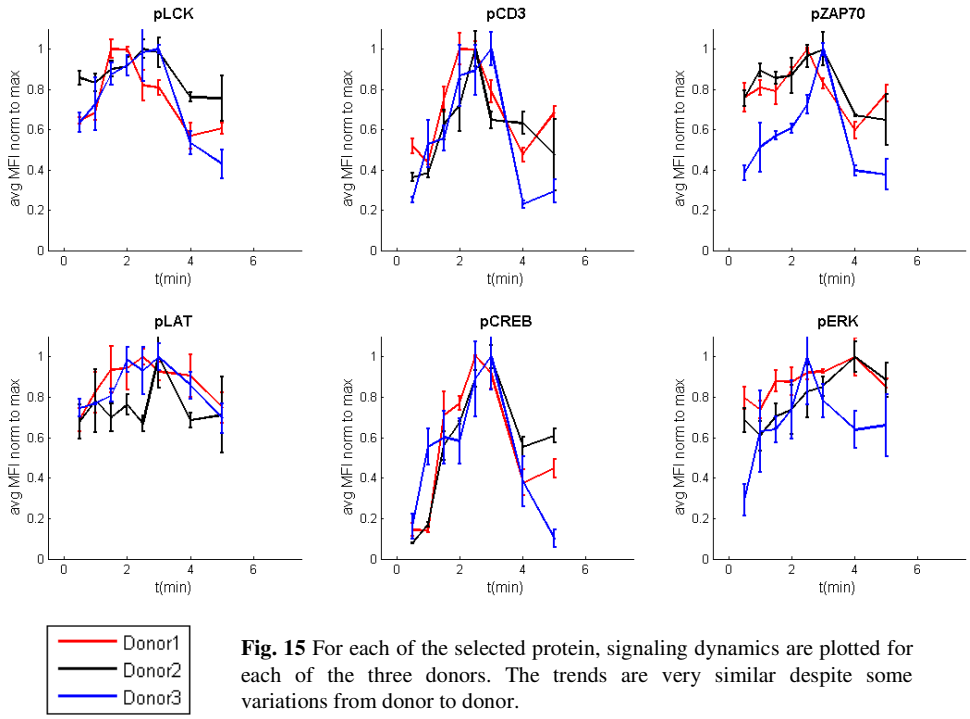

Fig. 15 For each of the selected protein, signaling dynamics are plotted for each of the three donors. The trends are very similar despite some variations from donor to donor.

We then compared the dynamics of primary T cells and those obtained with Jurkat cells (Figure 16). Although there are some differences in the magnitude of the response, the activation times and the dynamic trends are conserved from the immortalized cell line to primary T cells. For example, peak phosphorylation of CD3 occurs at 3 minutes and peak activation of Erk occurs at 4 minutes across all samples. As all the protein activation data are normalized to their maximal value, we can see that the basal levels of LCK, ERK and LAT are higher in primary T cells than in the immortalized cell line. CREB seems to dephosphorylate immediately after it reaches its activation peak at 4minutes in primary T cells, whereas in Jurkat cells it stays active for at least one more minute.

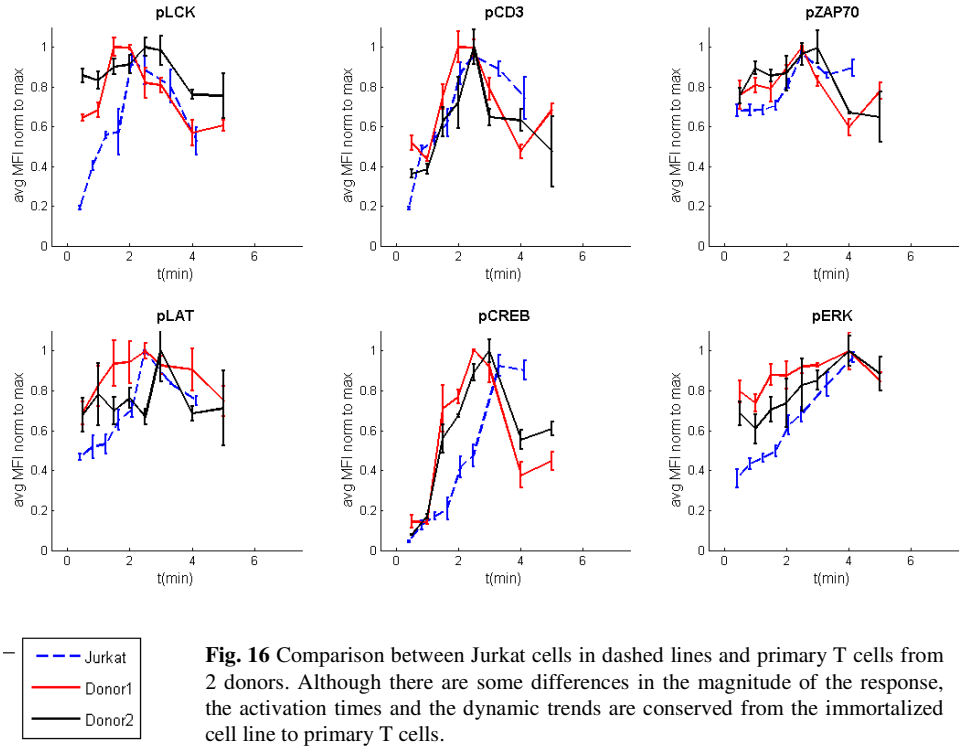

Fig. 16 Comparison between Jurkat cells in dashed lines and primary T cells from 2 donors. Although there are some differences in the magnitude of the response, the activation times and the dynamic trends are conserved from the immortalized cell line to primary T cells.

Mis en forme : Retrait : Première ligne : 1,06 cm

3.3 Cell senescence determination

3.3.1 Background

Adoptive transfer therapy relies on large quantities of T cells that maintain effector function. Because the adoptive transfer of senescent cells will result in suboptimal outcomes, a standardized method that can quantitatively evaluate the sensitivity of T cells to antigenic cues will improve the consistency of immune-based therapies in cancer treatment.

After a certain number of days of cultures, cells become anergic by senescence, and do not respond to antigenic cue. The production of IL-2 is decreased, and the levels of anti-apoptotic protein bcl-2 are low. Recently, Mazzati et al identified profilin-1, a ubiquitous protein associated with actin remodeling

and cellular motility, as an unambiguously identified protein that gets overexpressed in senescent T cells (2007).

It has been shown that anergic T cells have a weakened TCR response. ERK and JNK are known to be dampened. The block in the pathway of MAPK occurs before RAS but it is not known exactly which protein plays the major role.(Howe *et al* 2003)

3.3.2 Methods, results and discussion

Cell senescence could be observed in the regular culture. After 20 days of culture, without restimulation, the growth rate started to decrease, and the number of apoptotic bodies to increase in the culture medium.

To obtain quantitative data of senescence, we used profilin-1 as a biomarker. Every third day, 2 million cells from donor 3 were fixed with a 2% paraformaldehyde solution and 90% methanol and immunostained for profilin-1 (Cell Signaling). The levels of fluorescence of profiling were determined by flow cytometry (Figure 17). The data shown are the average of three different experiments. We observe a large increase on the 17^{th} day (Figure 17) and then at the 20^{th} and 22^{nd} day the levels of profilin are very low. This observation could be explained by the fact that cells started to die. The growth rate was almost null, and a quick experiment by flowcytometry showed two distinct populations of cells from day 20.

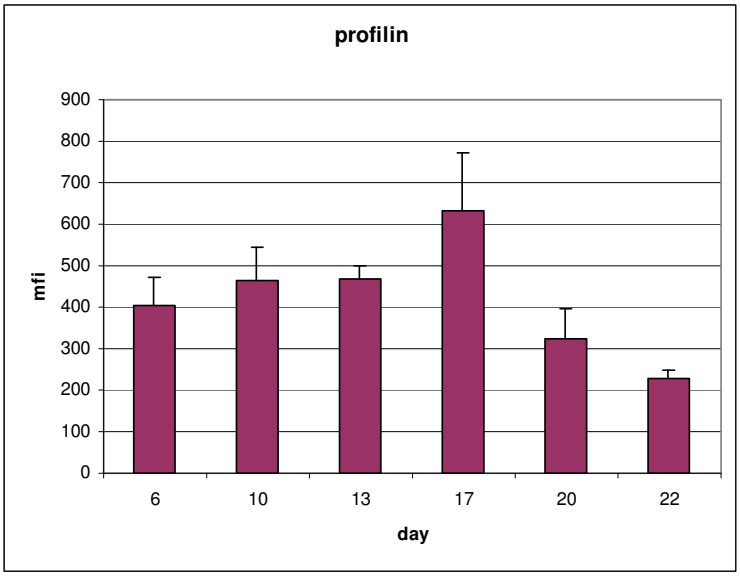

Fig. 17 Profilin is overexpressed in long term cultured cells. Primary T cells from a single donor were fixed, immunostained and visualized by flowcytometry.

To demonstrate the feasibility of using the microfluidic chip to compare the responsiveness of short term versus long term cultured cells, we measured protein activation dynamics for cells from donor 3 after 6 days and 16 days of culture. pCD3 and pZAP70 showed the maximal dampened response as shown in Figure 18.

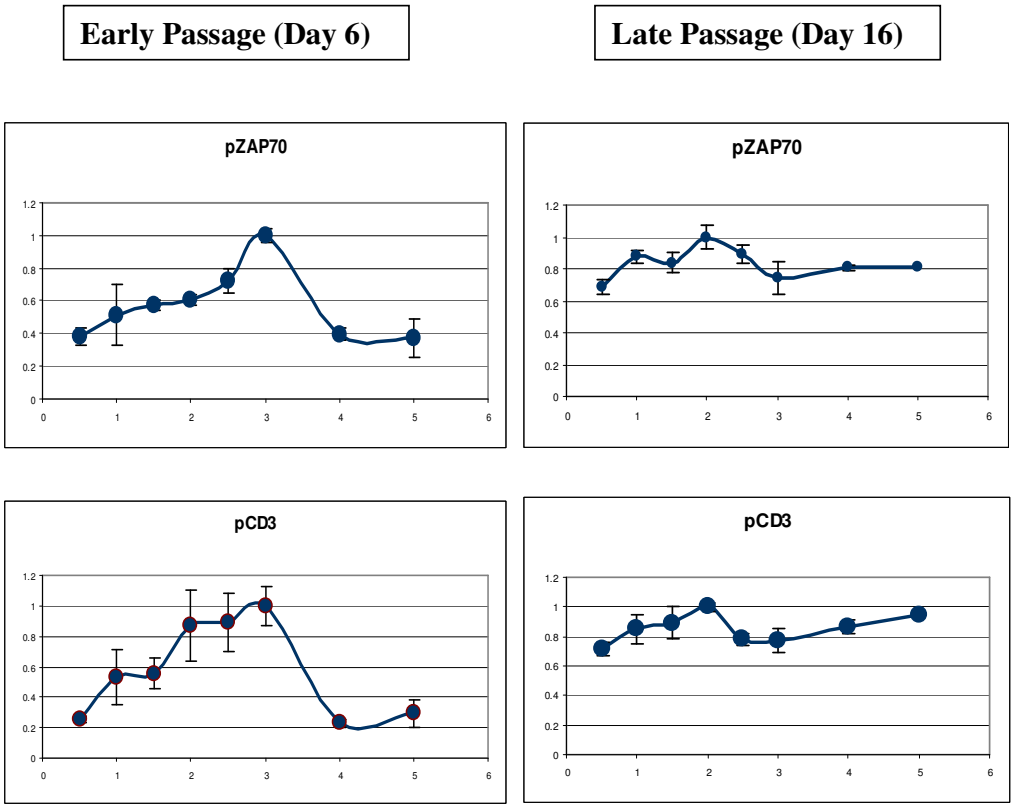

Fig. 18 The activation dynamics of pZAP70 and pCD3 are weaker in older cells. 8 millions cells from the same donor were flown through the microfluidic chip at day 6 and 16, and protein activation dynamics were quantified using the regular Luminex assay.

Further investigations within the expansion methods and different culture time could enable the creation of a discriminanting model that could quickly assess the degree of senescence of a population. Protein activation data for different stages of culture, as well as profilin-1 expression and IL2 secretion would be the input data.

Mis en forme : Retrait : Première ligne : 1,06 cm

3.4 A chip for fixing cells

The microfluidic chip has been so far used to mix cells with stimulus and then lyse cells to perform downstream analysis on the protein components. Imaging techniques or flowcytometry are also good

ways to observe some cellular behaviors, and it would be very interesting to take advantage of our quality stimulation resolution for use in other analysis techniques. Analysis of protein activation by flow cytometry requires a tedious fixing and staining process. Using the second module of the chip as a fixing module instead of a lysis module, we have progressed through an automation of the immunostaining process. To our knowledge, this is the first reported application of cell fixing on chip.

3.4.1 Methods

16 million T cells from donor 3 were harvested and resuspended in serum, phenol red free medium, supplemented with 7% dextran. Half of the cells were flowed through the microfluidic device with stimulus and lysis buffer. Lysates were collected, protein yield quantified with a BCA assay kit and phosphorylated proteins quantified with a Luminex based assay. The other half of the cells was flowed in another microfluidic device with stimulus and a 2% paraformaldehyde solution. It may be also possible to use the same chip to perform both lysis and fixing, by just exchanging syringes during the experiment and waiting for steady state before collecting to prevent cross-contamination of reagents. After collection of the fixed cells, they are centrifuged at 1500 rpm for 5 minutes, at 4°C, and resuspended in 90% methanol. As the method used later is based on single cell analysis, we did not perform any normalization to cell number. The fixed and permeabilized cells can then be stored at -20°C before further experiments. We chose to compare the dynamics of pERK and pZAP70 by these two methods. We used 4 aliquots for the immunostaining, 2 for each protein

3.4.2 Results and Discussion

As shown in Figure 19, the dynamics observed with both methods correlates well with each other. The minimum values seem to be lower with immunostaining. . We assumed that the cell distribution difference between the outlets was not broad enough to require a different concentrationantibodies and different volumes. Each sample was resuspended in 400 µl of methanol. However, we know from the

predictability of the cell distribution that in outlets 4 and 5, which corresponds to the smaller time points, 30 seconds and 1 minute, that the cell concentration is lower. The dilution factor can maybe explain this difference. We can also notice that the error bars are smaller with the Luminex based assay.

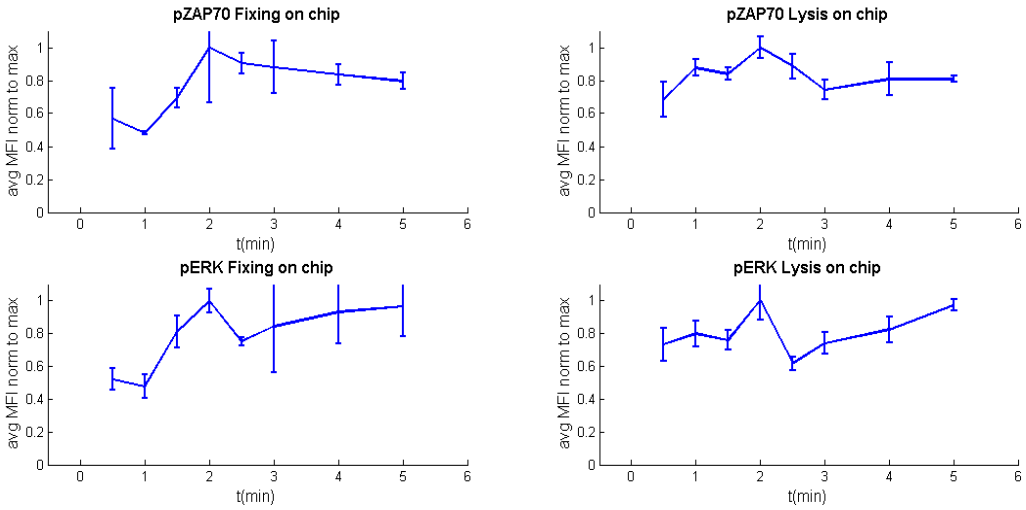

Fig. 19 The activation dynamics of pZAP70 and pERK were captured by lysing on chip and luminex bead based assay, and compared to the dynamics of these same proteins captured by fixing on chip and futher immunostaining. Both assays give very similar trends.

CHAPTER 4

CONCLUSION AND FUTURE WORK

Our device successfully accomplishes the tasks of multi-time point stimulation with on-chip cell lysis. Rapid mixing, achieved with the staggered herringbone array, allows precise time point resolution down to 20 seconds. Modeling and confocal mixing experiments gave valuable insight into the mixing of solutions, with a wide range of fluidic properties relevant to biological experiments. The flexible nature of this modular design allows easy adjustment of time points without changing the device or operation conditions. This one-time-use device is inexpensive to fabricate, simple to set up, and simple to use. The flexibility and potential for automation in the microfluidic format allows for future development for more "online" processing of samples, which may further reduce necessary sample volumes and cell concentrations. From a single experiment, 6 proteins were analyzed simultaneously for 8 timepoints, yielding 48 measurements from only 8 million cells, only 5% of the amount needed in conventional methods. TCR signaling dynamics were acquired with a very good time resolution and low sampling error compared to manual pipetting. A comparison between Jurkat cells and primary T cells showed very similar trends among these two populations across the 6 proteins. The modularity of the device was demonstrated by the unlimited range of time points that can be acquired but also by the usability of the second module, as a fixing or lysing chip. Comparison of activation dynamics for cells fixed on chip and then immunostained, and cells lysed on chip, whose lysates were incubated with antibody capture beads, shows very similar trends, even with different capture antibodies.

This microfluidic device also shows a great potential to study cell senescence. Adoptive transfer therapy requires a high quality expanded cell population before reintroduction into the patient. The

study of early signaling events in T cells with this device demonstrates excellent potential towards this goal. We have shown weakened protein activation after TCR ligation for long term cultured cells. A more in depth study of the magnitude of the activation state, correlated to biomarkers of senescence, such as the cytoskeleton protein profilin-1, or the magnitude of IL-2 secretion, can lead to the creation of a discriminant model enabling to assess quickly the state of senescence of a population. This study could include parameters such as type of expansion (IL-2 supplemented media only, IL-2 and CD3/CD28 beads), passage number, time of restimulation in culture, CD4+ vs CD8 T cells. This investigation could have a large impact on the clinical feasibility of adoptive transfer therapy and also on the scientific research population that needs to culture primary T cells.

APPENDIX A

Parallel multi-time point cell stimulation and lysis on-chip for studying early signaling events in T-cell activation

Alison Hirsch[a], Catherine Rivet[b], Boyang Zhang[a], Melissa Kemp[b,c,d], and Hang Lu[a,b,c]*

Received (in XXX, XXX) 1st January 2007, Accepted 1st January 2007
First published on the web 1st January 2007
DOI: 10.1039/b000000x

Dynamics of complex signaling networks are important to many biological problems. Quantitative data at early time points after cellular stimulation are necessary for accurate model generation. However, the large amount of data needed is often extremely time-consuming and expensive to acquire with conventional methods. We present a two-module microfluidic platform for simultaneous multi-time point stimulation and lysis of T-Cells for early time point signaling activation with a resolution down to 20 seconds using only small amounts of cells and reagents. The key design features are rapid mixing of reagents and uniform splitting into 8 channels for simultaneous collection of multi-time point data. Chaotic mixing was investigated via computational fluid dynamic modeling, and was used to achieve rapid and complete mixing. This modular device is flexible - with easy adjustment of the setup, a wide range of time points can be achieved. We show that treatment in the device does not elicit adverse cellular stress in Jurkat cells. The activation of 6 important proteins in the signaling cascade was quantified upon stimulation with a soluble form of α-CD3. The dynamics from device and conventional methods are similar, but the micro device exhibits significantly less error between experiments. We envision this high-throughput format to enable simple and fast generation of large sets of quantitative data, with consistent sample handling, for many complex biological systems.

Introduction

Understanding the dynamics of cell signaling networks is important to many biological applications, especially in complex disease phenotypes related to cancer, immune responses, development, and potential pharmacological interferences. Pathways involved in cell maintenance and apoptosis are studied extensively to understand cancer development[1, 2]. Focus on particular signal-transduction cascades and molecules has provided system-level insights into mechanism-based drug discovery[3, 4]. Building a system-level computational model and gaining insights in to the complex signaling networks requires large data sets, presently a bottleneck in the process. For example, gene expression patterns or protein activity at various time points during stimulation with an external signal must be known; it usually takes many labs years to accumulate a large body of this type of data[5-7]. Another challenge in signaling research is that many of these important protein activation events, such as phosphorylation, occur within minutes after stimulation[8-10]. Quantitative data not only at precise time points but early in the cells' response are necessary for accurate model generation.

Intracellular immunostaining techniques via flow cytometry have proven useful for studying signaling pathways[11]; however the multi-laser cytometers are constrained for the number of proteins monitored. Cell lysis and biochemical detection of population averages remains the most widespread method of capturing intracellular signaling dynamics of protein pathways. To extract the necessary protein information the cell must be stimulated for a precise period of time and immediately lysed to extract intracellular proteins for downstream analysis. With conventional, multi-well plate assays it is difficult to achieve adequate resolution at sub-minute timescales. Microfluidics is a capable alternative, providing uniformity in sample handling to reduce error between experiments. Moreover, microfluidic systems require relatively small sample volumes for experiments, conserving valuable cells and reagents[12]. Many microdevices have been reported for culturing cells, stimulating with soluble factors, assaying gene expression and performing lysis[13-22].

The challenges of any on-chip assays are that the devices should minimize stress on the cells, should provide reproducible results from experiment to experiment, should produce quantitative results comparable to or better than bench-top schemes, should be scalable to high throughput format, should minimize consumption of cells and reagents, and ideally provide the temporal resolution that the bench-top counterparts cannot achieve. So far no chip-based designs have achieved all these criteria simultaneously. Here we present a lab-on-a-chip platform for multiple time-point lymphocyte stimulation and lysis for downstream analysis of protein activation. Mixing and even splitting of reagents into each time-point channel are key features of the design.

Previously El-Ali *et al.* developed a device achieving cell stimulus and lysis on a microfluidic chip using segmented

gas-liquid flow for rapid mixing[16]. This device was the first to demonstrate on-chip multiple step manipulation of cells with fast mixing, thereby allowing access to the early time-point detection of protein states. For our application however, to understand over time how multiple proteins in the signaling network behave upon stimulation, vastly different incubation

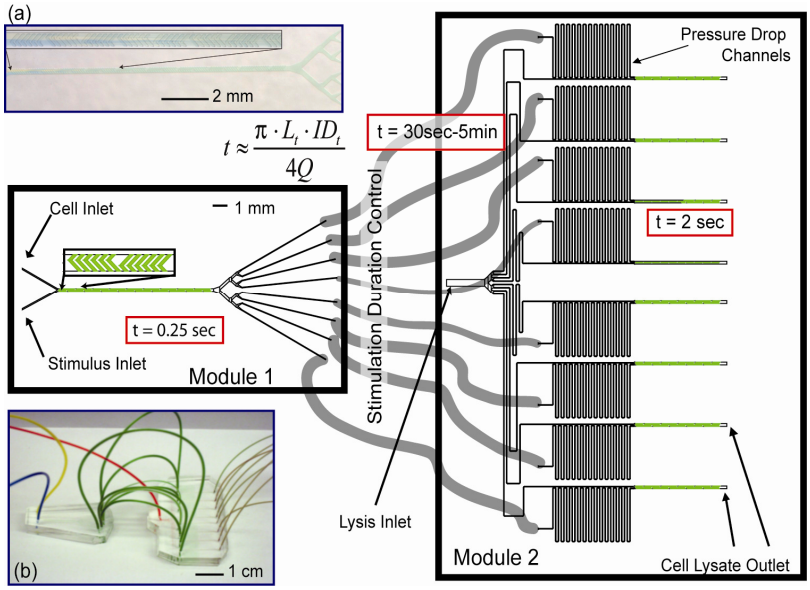

Fig. 1 A schematic of the devices showing inlets, tubing, pressure drop channels and cell lysate outlets for sample collection. The respective residence times (t) in each unit are noted in red boxes on the figure, where the total time is essentially the time in the tubings, varying with length (L), inner diameter (ID) and volumetric flow rate (Q). Insets (a) shows a close-up of Module 1 and (b) the whole device setup.

periods are required. Therefore we have designed our device for 8 time points in parallel with controlled rapid mixing, precisely timed stimulation, and rapid lysis. In addition, in this work we also circumvent the large shear at the gas-liquid interface in the earlier work. We show that our assay platform does not induce stress responses to the cells and yields reproducible and quantitative protein activity information with small numbers of cells.

Experimental Design

In order to achieve precise incubation control on multiple time scales, we took a two-module approach for increased system flexibility (Figure 1). In our design, pressure-driven flow (by syringe pumps) entered at only 3 inlets -- cells, stimulus and lysis buffer -- which made handling multiple samples and parallel experiments simple. Cells and stimulus were mixed and split into 8 equal streams in less than 0.25 seconds on Module 1. The majority of the incubation time (~20 seconds to 5 minutes in our experiments) occurred in the tubing leading to Module 2. On Module 2 the reaction was quenched and cells were lysed by mixing with cold lysis buffer, in less then 1 second, to extract intracellular components. Mixing and balancing flow-rates were important to the design, which we describe below.

Rapid mixing to ensure precise stimulation times

For precise definition of stimulation time, especially for the very early time points (e.g. 20 seconds), rapid mixing of cells with reagents was essential to our design. Mixing is necessary in multiple steps of the assay: the cells first have to be mixed with the stimulant, and then once incubated for the desired duration they have to be mixed again with lysis buffer to yield lysate for downstream biochemical assays. If mixing takes a significant portion of the time compared to stimulation and lysis incubation, cells suspended in the initial medium will be introduced to the stimulant at different times, and the contact time cannot be precisely controlled. This non-uniformity of contact time would make it difficult to define and repeat the "stimulation time".

We considered a few existing designs of microfluidic mixers. El-Ali *et al* have shown a gas/liquid segmented flow scheme to enhance mixing[16]. The advantage of this mixing scheme is that it is very fast and the throughput is high; however, because the mixing scheme relies on the circulation of the liquid behind gas bubbles, the shear is large at the multiphase interface and can introduce undesired lysis and/or mechanotransduction in cells. Ugaz *et al.*[23] demonstrated Dean flow mixing, which is simple and could be suitable for many biological experiments since it is gentle. However, for Dean flow mixers, better mixing correlates to higher Reynolds' numbers ($\mathrm{Re} = \rho \cdot v \cdot L/\mu$ where ρ is the density of the fluid, μ the viscosity, v the linear velocity, and L the channel's limiting dimension, is a measure of the inertial effect over viscous effect of fluid flow). To implement this

mixing scheme for our application would require large flow rates that render the subsequent incubation step impractical. We chose the asymmetric herringbone mixer (HBM)[24]. The mixing time in these devices are sufficiently short for our application and the shear is minimal. There is no analytical solution to the mixing scheme, and a limited number of experiments have been performed on such mixer designs[25-27]. Optimized parameters, asymmetry of the herringbones (2/3 of the way across the channel) and angle with respect to y-axis (45°), from Stroock *et al.* were used as a starting point in this design[24].

In order to design proper mixers for our application and determine an accurate starting time of incubation, we developed computational fluid dynamics (CFD) models for different geometries and experimental flow conditions using COMSOL (Stockholm, Sweden), a finite element solver for non-linear partial differential equations. Because our buffers, cell solutions, and stimulation solutions can have different fluidic properties, the model was also used to probe the mixing effects of viscosity and density. Further confocal microscopy experiments were used to visualize the mixing of solutions with mismatched viscosity.

Flow splitting and precisely-controlled stimulation

After mixing, the fluid was split into 8 streams on Module 1. Each stream accomplished a different time point in the tubing leading to Module 2. For efficient device operation, it was necessary for equal volumes of sample to be collected for each time point. Equal flow rates in each stream were achieved by balancing the channel resistance. The resistance, proportional to fluidic pressure drop and a function of channel dimensions, increases with increasing length and decreasing cross-sectional area. From the Hagen-Pouseille equation,

$$\Delta P = \frac{128\mu \cdot Q \cdot L}{\pi \cdot d^4} \quad (1)$$

where ΔP is pressure drop, μ is viscosity, Q is volumetric flow rate, L is path length, and d is the diameter, we calculated a relationship for resistance (R) based on channel dimensions.

$$R \propto \frac{L}{d^4} \quad (2)$$

Since the microfluidic channels are square, when implementing these equations a hydrodynamic diameter was used,

$$d = \frac{2(h \cdot w)}{h + w} \quad (3)$$

where h is the channel height and w is the channel width. This hydrodynamic diameter definition neglects the effect of channel shape,[28] but suits our application in determining the order of magnitude resistance differences between tubing and channels. All the lengths and widths of the are the same in each time point channel to achieve equal resistance.

The stimulation time is defined by residence time in the device. This time is the sum of the residence time in the channels and the residence time in the tubing leading to the lysis module (Module 2).

$$t = \frac{L_c h_c w_c}{Q} + \frac{L_t \pi \cdot ID_t}{Q} \quad (4)$$

The subscripts c and t denote channels and tubing, respectively, and ID is the inner diameter.

This modular design, as shown in Figure 1, created a more flexible system by using interchangeable tubing of different lengths and diameters for multiple time point options. The majority of the incubation time occurred in the interchangeable tubing. However, the flow rates must not be influenced when changing lengths or diameters of tubing. This is inherent in out system design because of the small dimensions of the microfluidic channels and the d^4 dependence in the denominator in Equations 1 and 2. In the worst case scenario with dimensions used in our experimental setup, the channel resistance was still four orders of magnitude greater than that of the tubings. Furthermore, additional long pressure drop channels were added to increase this effect. Small variations in the channel dimensions in the PDMS molding should not effect our flow distribution and residence time predictions. Since each time-point channel has the same dimensions, the major importance relies in the relative difference between the channels and tubing. This order of magnitude effect will not be influenced by micron-sized variations in the device fabrication process. To ensure this premise holds, the flow rates at each outlet were measured experimentally and validated.

Materials and Methods

Device Fabrication

This two-module device was fabricated using standard soft lithographic techniques[29]. Briefly the modules were molded in poly(dimethyl-siloxane) (PDMS) (Dow Corning Sylgard 184, Essex-Brownwell Inc., McDonough GA) from a two-layer SU-8 (Microchem Corp., Newton, MA) master. One layer of 50 µm thick SU-8 2050 was spun onto 100-mm silicon wafer, baked, and exposed under UV light to define a negative image of the channel system in the resist. After baking to crosslink the exposed resist, another layer of 15 µm thick SU-8 2010 was spun on top. This layer formed the staggered herringbone array. After the same bake and expose process, the wafers were developed using propylene glycol monomethyl ether acetate (Doe & Ingalls, Inc., Durham NC). The wafer was surface-treated with vapor-phase tridecafluoro-1,1,2,2-tetrahydrooctyl-1-trichlorosilane (United Chemical Technologies, Inc, Bristol PA) for surface passivation. Then PDMS was cast on the SU-8 master and baked for 2 hours at 70 °C. The PDMS was peeled off the mold and individual devices were cut to size. Medical grade polyethylene (PE) tubing (Scientific Commodities, Lake Havasu City, AZ) of various lengths and inner diameters were used to for fluidic connections. Holes for fluidic connections were punched to a size determined by the outer diameter of the appropriate

tubing.

Device operation

A syringe pump (Harvard Apparatus PHD 2000 Series Infusion) controlled the flow to the 3 inlets at 28.22 µL/min resulting in a 1/2 dilution of the stimulus and a 1/3 dilution of the lysis buffer. Because of this, the stimulus and lysis buffer were delivered at 2x and 3x concentration, respectively. The input cell concentration was ~$8x10^6$ cells/mL. The resulting sample flow rates were 10.58 µL/min. For negative control, cell culture medium was first used in the place of the stimulation solution. After the start of the flow, the fluid was flushed to waste for 9 minutes before sample collection. The time corresponded to that for the fluid front to get from the syringe to the end of the outlet tubing. The sample lysate effluent was collected for approximately 15 minutes to obtain 150 µL of sample, enough to perform all downstream analysis. To stimulate the cells, the process was repeated, with 2 µg/mL OKT3 antiCD3 diluted in media in place of cell culture medium inlet. The total amounts of reagents used for all 8 time-point sample collections included only 1.35 mL of cell suspension and lysis buffer, and 0.68 mL of media and stimulus. With improvements on the sensitivity of downstream analysis it is possible to collect far less lysate, thus conserving valuable sample.

Cells tend to settle over time because they are denser than the media that they are suspended in. The settling in the syringes and tubings causes cell loss during experiments and unreliable time data. Settling in the microfluidic channels causes the cells to roll along the bottom of the channel rather than follow the streamlines. To resolve this issue, the media and stimulation solutions were supplemented with dextran of ~70,000 MW (Sigma-Aldrich) to match the density of the cells (approx. 1.07 g/cm^3). The cell distribution after Module 1 was characterized by using only Module 1 with one inlet flowing medium containing cells at a know concentration and the other medium, both supplemented with dextran. The suspension in each outlet was collected and cells were counted to determine cell concentration.

Confocal microscopy

The confocal experiments were performed on a LSM 510 UV microscope (Carl Zeiss Inc) with a 20x lens. Rhodamine-B dye at 0.05 mg/mL was used in one of the two entering streams. Inlets were perfused with the same flow rate as experimental conditions. The mismatch viscosity was created by using solutions of sucrose in water[30].

Excitation was from a helium-neon laser (543 nm, 0.5 mW) and emission at 560 nm using a long pass wavelength filter optimized for Rhodmine-B. The pixel time was 1.6 µs with 2-µm slices in the z plane. Confocal images were used to evaluate the extent of mixing. After each cycle the standard deviation (σ) of intesity distributions of the channel crossections. A σ value of 0.5 signifies completely unmixed streams while a 0 value signifies completely mixied streams. For figure clarity the brightness and contrast were increased in the same way for all x-y projections.

Computational Fluid Dynamic Models for the Chaotic Mixer

We modeled the transport and mixing in the HBM using the 3-D Navier-Stokes equations for flow and the diffusion-convection transport equation for the stimulant and the lysis buffer components at steady state. These equations were solved using COMSOL. Because of the asymmetry in the HBM, the model could not be reduced. However, the Navier-Stokes and convective diffusion equations can be decoupled and were solved separately. The vector form of the Navier-Stokes equations was as follows:

$$\rho\frac{\partial \mathbf{u}}{\partial t} - \mu\nabla^2\mathbf{u} + \rho(\mathbf{u}\cdot\nabla)\mathbf{u} + \nabla p = F \qquad (5)$$

where ρ is the density, μ is the viscosity, $\boldsymbol{u}$ is the velocity vector, p is pressure, and F is a volume force field (gravity).

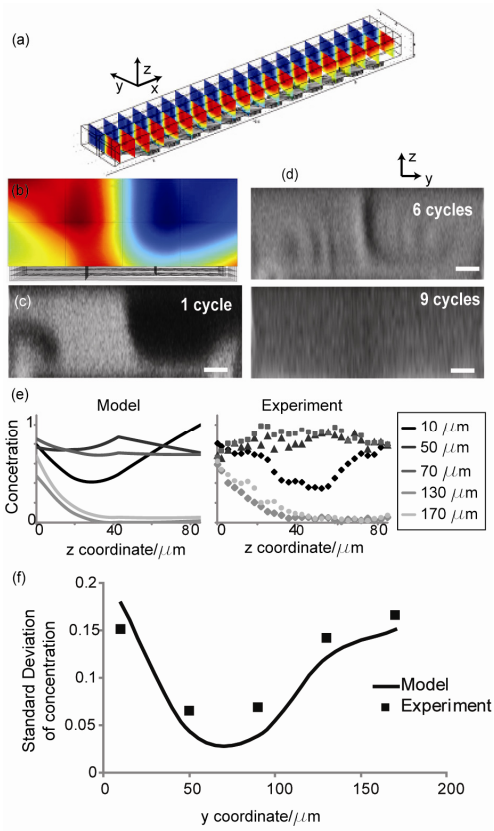

Fig. 2 Comparison of COMSOL model results with experiment. (a) perspective view of the mixing for 1 cycle of herringbone mixers. The slices are in the y-z plane perpendicular to the direction of flow. (b) y-z plane of the concentration profile color map from the model after 1 cycle. Under the color map the z component of the herringbones are illustrated. (c) y-z view of a confocal image of mixing after 1 cycle with one inlet containing rhodamine dye. (d) y-z mixing profile after 6 and 9 cycles.

The scale bar is 20 µm, twice the average diameter of a T-cell. (e) comparison of mixing profiles at in the cross section. Each line represents the normalized concentration profile in the z direction at the designated distances in the y direction from the wall. (f) standard deviation of concentration across each line in (e).

This solver assumes incompressible flow ($\nabla \cdot \mathbf{u} = 0$). The boundary conditions were assigned as parabolic flow profiles at a given average velocity for the inlets, zero pressure at the outlet, and non-slip on all remaining exterior boundaries. The interior boundaries, were all assigned a neutral condition. These interior boundaries were created for enchanced 3-D mesh resolution by splitting the flow channel into 8 subdomains and the herringbones into 6 subdomains each. This created additional nodes inside the subdomain while allowing a continous solution to the Navier-Stokes equations. The mesh density was such that further increases did not effect the convergence of the solution. The final mesh consisted of 65,000 elements with average quality >0.3.

Then using the velocity field from the solution of the Navier-Stokes equations, the non-conservative convective diffusion equations were solved

$$\delta_{ts} \frac{\partial c}{\partial t} + \nabla \cdot \left(-D\nabla c\right) = R - \mathbf{u} \cdot \nabla c \qquad (6)$$

where δ_{ts} is the time-scaling coefficient, equal to 1 when solving in the seconds timescale (this term will drop out at steady state), c is the concentration, D is the diffusion coefficient (~1×10^{-11} m^2/s for protein molecules[31]), R is the reaction rate (set to zero in our model), and $\boldsymbol{u}$ is the 3-D velocity profile from the Navier-Stokes equations. The boundary conditions were assigned as $c = 1$ and $c = 0$ at each inlet, convective flux at the outlet, and insulation at all remaining exterior boundaries. The interior boundaries were all assigned a continuity condition.

Cell Culture, Cell Lysis and Protein Analysis

For this study, we used Jurkat E6-1 human acute T-cell lymphoma from ATCC (Manassas, VA, USA). Cells were cultured in RPMI 1640 medium with L-glutamine (Sigma-Aldrich) with 10 mM HEPES, 1 mM Sodium Pyruvate, and 1X MEM Nonessential Amino Acids, and 100 units/mL penicillin streptomycin (Cellgro), supplemented with 10% certified heat inactivated fetal bovine serum (Sigma-Aldrich) at 37 ºC in a humidified 5% CO_2 incubator. For the experiments, Jurkat cells were resuspended in a phenol-red free RPMI 1640 medium (Sigma-Aldrich), supplemented with the previous reagents and 0.3 mg/ml of L-Glutamine (VWR) and 7 wt% dextran (Sigma-Aldrich). For the cell signaling experiments, the cells were treated with anti-human CD3, clone OKT3 (eBioscience) at a final concentration of 2 μg/mL. The lysis buffer used in these experiments was based on a 1% NP-40 solution (USBiological), supplemented with 1 M β-glycerophosphate (Calbiochem), 0.2 M sodium pyrophosphate (Alpha Aesar), 1 M sodium fluoride (EMD), 5 M Tris (Promega), 0.2 M sodium orthovanadate (Alfa

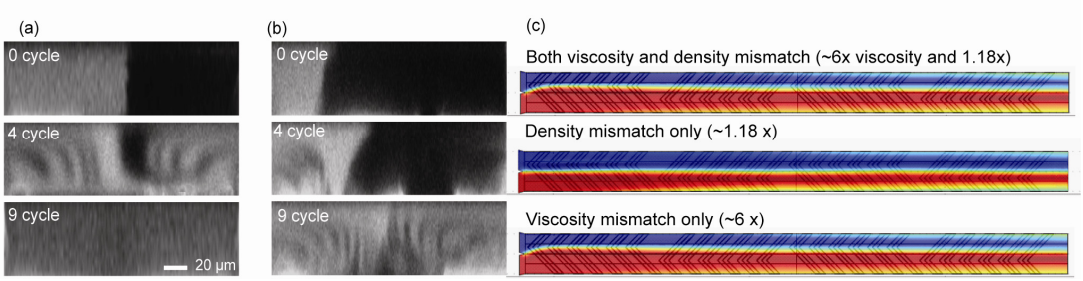

Fig. 3 Comparison of mixing of different viscosity solutions. (a-b) Confocal images of the cross section at increasing mixing cycles of herringbones. One inlet contains fluorescent rhodamine dye. (a) y-z cross-sectional view of the mixing of two fluids with the same viscosity. (b) y-z cross-sectional view of the mixing of two fluids with mismatched viscosity; the fluid with no fluorescent dye has a viscosity 20 times the other. (c) top view in the x-y plane of COMSOL data for density and viscosity mismatched solutions. The viscosity and density values are based on the sucrose solutions used with 6x the viscosity of water.

Aesar), 5 M sodium chloride (Alfa Aesar), 100 mM benzamidine (Sigma), 500 mM EGTA (VWR), 5 mg/ml aprotinin (Sigma), 5 mg/ml leupeptin (VWR), 1 mg/ml pepsatin (Sigma), 1 mg/ml microcystin-LR (Sigma). For device-mediated cell lysing, lysis buffer at 0 °C was directly mixed with the cell suspension in Module 2 and lysate solution collected at the outlets of the device in microcentrifuge tubes. For standard bench lysing, the addition was made by pipette addition of lysis buffer to microcentrifuge tubes containing the cells. For both forms of lysing, the samples were incubated on ice for 10-30 minutes, centrifuged at 14,000 rpm for 10 minutes and the supernatants were used for further analysis. The total protein concentration after lysis was determined with a BCA assay kit[32] and results were obtained after protein content between samples was diluted to uniform levels.

Stress and Signaling

All analysis of phosphorylation dynamics were performed with a Bio-Plex-200 instrument (Bio-Rad) using commercially available Luminex bead assays. The phospho-JNK and phospho-p38 measurements (BioRad) or the quantification of proteins downstream of TCR (Beadlyte 7-plex Human T-Cell Receptor Signaling Kit, Millipore) were completed according

to manufacturers' protocols. Results for all data are presented as the average of three independent sets of experiments. To adjust for baseline changes between experiment days, mean fluorescence intensity for each protein assay across samples was normalized by the maximum value for the data.

Results and Discussion

Analysis of rapid mixing by microscopy and computational methods

The CFD modeling results and confocal images from experiments are shown in Figure 2. In the confocal images (Figure 2 c and d), the bright fluorescent fluid is analogous to a stimulus rich solution and the dark areas is analogous to fluid with no stimulus. The experimentally determined profiles are similar to those by Stroock *et al.* under the same conditions. More importantly, the computational model agrees well with experimental data (Figure 2 e and f); hence the models can be used as a tool to probe the mixing properties and factors that may influence the extent of mixing to optimize our experimental conditions. Experimental results for mixing of solutions with the same viscosity (mimicking cell and stimulus mixing conditions) suggest that most cells would come into contact with the stimulus after 6 cycles because the widths of the stimulus-negative solution stream are smaller than the cell diameter (~ 10 μm); the standard deviation of mixing is 0.14. After 9 cycles the solutions are completely mixed with a standard deviation of 0.05.

In contrast, when solutions with mismatched viscosity and density are mixed (as in the case of mixing cell suspension, $\mu \sim 4.3$cP and $\rho = 1.07$g/cm^3, with lysis buffer,$\mu \sim 2.4$ cP and $\rho = 1.06$ g/cm^3) with the same HBM, as seen in Figure 3, the streamline profiles and hence the extent of mixing are qualitatively different. In this case, the mixing is slower and less efficient, marked by incomplete mixing after 9 cycles in a mixing of solutions of 20 times viscosity mismatch. The standard deviation was 0.12. Although the viscosity and density of fluids are correlated in most cases, we can separate the two effects in the numerical simulations. Our models suggest that less effective mixing is mainly due to the mismatch in viscosity, not the difference in density, because the more viscous solution has a lower average velocity and therefore takes up more cross-sectional area (Figure 3c). This results in the fluid interface moving beyond the point of asymmetry (2/3 of the way across the channel) of the herringbones, reducing the effectiveness of the herringbones' ability to stretch, fold, and mix the two fluids. However, this effect occurs only at viscosity ratio of 6:1 and above for the current HBM design. Because we use dextran-supplemented solutions, we stay below the 6:1 viscosity ratio and therefore the HBM is adequate for fast mixing of cells and stimulus in Module 1, and of cells and lysis buffer in Module 2.

The model was also used to characterize the shear stress at the walls. At the channel wall, the highest shear stress is ~6 Pa and the highest shear stress at the herringbone wall is ~1.8 Pa. These numbers are on the same order as the in the blood, with maximum shear stress of approximately 4 Pa.[33]

Tight control of stimulation times in multiple parallel samples

Based on the channel dimensions and fluid flow rates of the optimized setup, the staggered herringbone array achieved full mixing of reagents with minimal shear in less than 0.2 seconds on the stimulation chip (Module 1), and <0.9 seconds on the lysis chip (Module 2). These times are less than 5 percent of the ~23-second stimulation time, which was the shortest stimulation time in our experiments. Hence the mixing time does not significantly affect our time point data.

Taylor dispersion, caused by diffusion and the parabolic flow profile, could be important for the cell stimulation time.

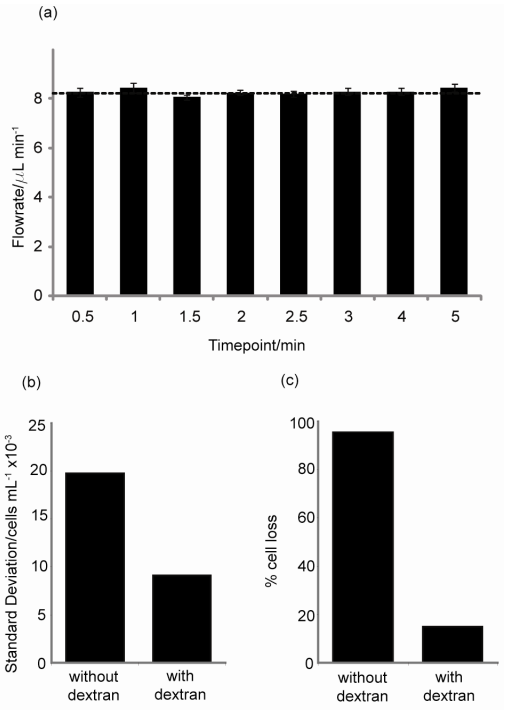

Fig. 4 Demonstration of device uniformity. (a) Equal flowrates in μL/min across the different channels. The channels are noted with the corresponding stimulation time in minutes. The dashed line indicates the set flow rate (total/number of channels) and error bars indicate standard deviation. (b) The average standard deviation of cell concentration in each stream with and without dextran supplement in the solutions. The standard deviation between experiments is decreased by half with the addition of dextran and percent cell loss is markedly decreased.

With a diffusion coefficient on the order of 10^{-10} cm^2/s (from Stokes-Einstein's equation), the modified Peclet number (ratio of the shortest residence time to the timescale for dispersion) is on the order of 10^5, suggesting that Taylor dispersion in the tubing will introduce errors in the stimulation/incubation time. However as we demonstrate in the protein signaling experiments in this work, the time points resolve easily and a trend can be quantified. If necessary, further experiments to determine the true residence time distribution can be used to

deconvolve such time-series data, or an alternative incubation strategy can be used. For example, mutliple chips with long channels of different volumes and also with integrated herringbone structures can be used in place of tubing, and may tighten the residence time distribution of the samples.

Flow resistance balance to achieve equal distribution of fluids

The flow rate in each outlet was characterized as described in the experimental methods section. Figure 4a shows the flow rates across different time points with varying tubing dimensions. Error bars represent the standard deviation from trial to trial, which demonstrates the repeatability from device to device. The flat trend and tight standard deviation around the target 8.3 µL/min flow rate demonstrates the reliability of the device flow rates even while varying length, widths, and thus resistance of the tubing (as shown it Table 1) between Modules 1 and 2 for each point. The highest pressure drops in the tubing is 66 Pa, as compared to 18 kPa in the microfluidic channels. The advantage is that this configuration provides large flexibility of the specific time points for stimulation we can achieve. With commercially available tubings, we can easily achieve stimulation times of ranging from ~20 seconds to 1 hour.

Table 1 Example tubing dimensions for given time points and the pressure drop (analogous to resistance) for each tubing.

Time point/min	Tubing ID/μm	Tubing Length/cm	ΔP/Pa
0.5	280	4.2	66.4
1	380	4.7	21.9
1.5	580	3	2.6
2	580	4.1	3.5
2.5	580	5.2	2.6
3	580	6.2	3.1
4	580	8.3	4.2
5	580	10.4	5.3

Reliable cell distribution after stimulation and reliable protein yield after lysis

Without adding dextran to the cell suspension, cells were often observed to settle and aggregate; these aggregations in turn cause blockage on chips and together with settling cause the cell distribution in the 8 collected samples to be non-uniform and unpredictable. In comparison, reliable cell distribution between experiments was achieved by adding dextran to the solutions for density matching. In addition, dextran may also contribute to the suppression of non-specific adsorption of serum proteins in the medium, which promotes cell adhesion to the device walls. As shown in Figure 4b, the average standard deviation of cell density in each stream was decreased by more than half. These data were obtained by flowing cells through the device at a known density, but replacing the stimulus and lysis solutions with media, and counting intact cells from each outlet. In addition, by taking the cells lost (Figure 4c) to settling in the syringes and devices into account, the resulting improvement by adding dextran is very significant. Although variability between cell concentrations per stream still exists, protein activity data can be easily normalized by the total protein in the sample. We have verified that the total protein yield is linearly correlated to the number of cells in the sample (data not shown).

On-chip cell handling showing minimal stress on cells

For a microfluidic device to perform optimally for signal transduction applications, fluid forces must not impose adverse stresses on the cells within the chip. To validate that the cells flowing through the device were not subjected to undesirable shear stress due to fluid flow in narrow channels, undesirable mechanical forces produced by chaotic mixing, or lack of oxygen perfusion during the course of the experiment, the phosphorylation state of two MAPK proteins associated with stress response, p38 and JNK, were monitored. Cells in dextran-supplemented medium (no stimulatory reagents) were pumped through Module 1 and lysed in Module 2. The lysates were compared to the results from cells lysed by an analogous bench-top protocol (also without any stimulation). As shown in Figure 5, the levels of p38 and pJNK activation for the on-chip experiment are constant over time and comparable to the results obtained on bench, demonstrating that the cells are neither adversely stressed by the conditions imposed by flow through the microchannels, nor stressed by the time spent in the tubings. There was no noticeable change in cell viability or morphology as observed by trypan blue exclusion after cells were subjected to flow through the device (data not shown).

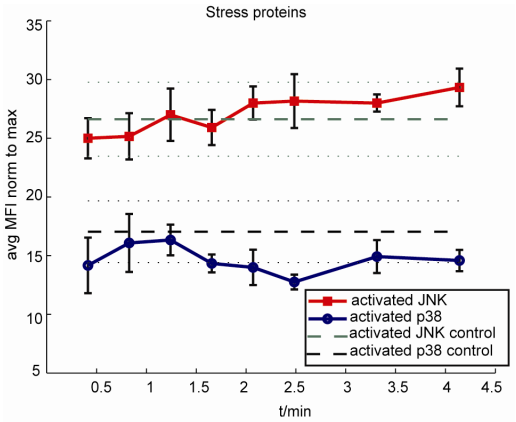

Fig. 5 Activated JNK and p38 concentrations in cells collected from the microfluidic devices compared to on bench controls, showing now signs of cellular stress induced by the device. For this experiment, samples were normalized to total cellular protein content. The experiments were run with three different devices and then the protein phosphorylation quantification was obtained with duplicates. Dashed lines represent the quantified values for phospho-p38 and phospho-JNK from control samples lysed on the bench. Dotted lines indicate standard deviation associated with the control values. Mean fluorescence intensity measurements for positive controls were comparable in magnitude to positive control lysates supplied by the manufacturer (data not shown).

Parallel on-chip experiments for high-throughput multi-time point protein activation assays

The temporal regulation of protein activation during T-Cell receptor signaling involves multiple coordinated feedback loops, as reviewed by Germain *et al.*[10]. Prior proteomic studies indicate widespread phosphorylation of signaling molecules occur within 5 minutes of T-Cell activation[34]; thus, a method for consistent generation of sub-minute signaling events would be useful for extracting relationships between interconnected network components. To ensure that the microfluidic system is a reliable method of evaluating T-Cell activation, we characterized the phosphorylation dynamics of representative signaling molecules downstream of the T-Cell receptor (Figure 6a). Comparisons between anti-CD3 (OKT3) stimulated Jurkat lysates generated by standard bench-top protocol and those generated by the device were made using the Beadlyte 7-plex human T-Cell receptor phosphoprotein signaling kit (Upstate). This kit quantifies phosphorylated ITAMs (CD3ε), ZAP-70, Lck, LAT, Erk, and CREB using the Luminex instrument as described by Khan *et al* [35]. Jurkat cells in a 7% dextran medium were stimulated with the soluble form of anti-CD3 for the incubation times ranging approximately from 20 seconds to 4.5 minutes and then lysed with a cold lysis buffer containing phosphatase and protease inhibitors that prevent further biochemical events after lysis. Figures 6b-6g show the signaling dynamics for these 6 proteins of interest for lysates generated by the microfluidic device and for lysates generated on bench. As illustrated in the simplified scheme of the TCR signaling cascade (Figure 6a), the first proteins to be phosphorylated are CD3, Lck and Zap-70. Multiple signaling events occur before the downstream adaptor LAT, and the kinases Erk and CREB, are phosphorylated.

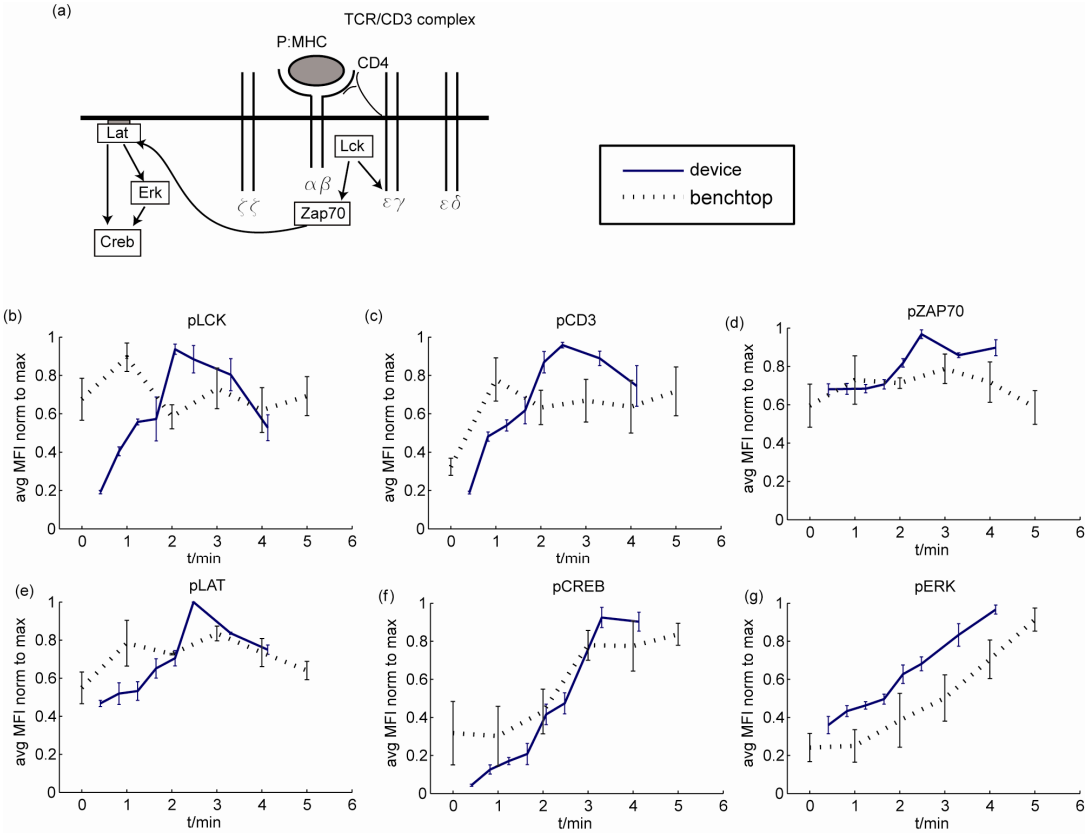

Fig. 6 (a) Simplified pathway of TCR activation. After a peptide MHC has bound to the CD3/TCR complex , Lck phosphorylates the ITAM CD3, that recruits the tyrosine kinase ZAP70 to the complex. Zap70 phosphorylates then the adaptor protein LAT that activates the MAPK and the Ras pathway, the latter enabling the activation of Erk and Creb. In our case, we used OKT3 that specifically reacts with the CD3 complex. (b-f) For each of the selected protein, comparison of the dynamics obtained with the microfluidic device and those obtained by standard bench top protocol. The dynamics are very similar and the microfluidic device shows a better consistency in the results.

With the device, phosphorylation of CD3, Lck and Zap-70 starts after 2 minutes of stimulation and reaches its peak at 3 minutes. In contrast, the phosphorylation of Erk rises concurrently with the downstream protein Creb over a longer period of 5 minutes. As expected, smaller variation occurs among samples across repeated experiments with the microfluidic device than with the manual stimulation and lysing, demonstrating a tight control over cell handling on-chip. The dynamic trends of activation are not dissimilar between the two experimental methods; however, an important feature emerges from the data. The uniformity of stimulatory exposure results in higher magnitudes of phosphorylation at early time points for all proteins measured. This is especially evident in the CD3 ITAM phosphorylation, possibly due to a flattened distribution of stimulated cells in the manual bench-top samples arising from the time lag of antibody:cell mixing. This feature highlights the necessity of consistent sample handling when quantifying cell population averages for signaling dynamics, especially when using small numbers of cells.

Conclusions

Our device successfully accomplishes a multi-time point stimulation experiment with on-chip cell lysis. Rapid mixing, achieved with the staggered herringbone array, allows precise time point resolution down to 20 seconds. Modeling and confocal mixing experiments gave valuable insight into the mixing of solutions, with a wide range

of fluidic properties, relevant to biological experiments. The flexible nature of this modular design allows easy adjustment of time points without changing the device or operation conditions. This one-time-use device is inexpensive to fabricate, simple to set up, and simple to use. The flexibility and potential for automation in the microfluidic format allows for future development for more "online" processing of samples, which may further reduce necessary sample volumes and cell concentrations. From a single experiment, 6 proteins were analyzed simultaneously for 8 timepoints, yielding 48 measurements from only 10 million cells, only 5% of the amount needed in conventional methods[7]. We expect a high-throughput format of this device coupled with multiplexed biochemical analysis to yield large sets of quantitative data for reconstructing signaling networks in many applications.

Notes and references

[a]School of Chemical. and Biomolecular Engineering, Georgia Institute of Technology
[b]Interdisciplinary Program in Bioengineering, Georgia Institute of Technology
[c]The Petit Institute for Bioengineering and Biosciences, Georgia Institute of Technology
[d]The Wallace H. Coulter Department. of Biomedical Engineering, Georgia Institute of Technology and Emory University
*Georgia Institute of Technology,School of Chemical & Biomolecular Engineering, 311 Ferst Drive, N.W., Atlanta, GA 30332-0100. Fax: 404 894 4200; Tel: 404 894 8473; Email: hang.lu@chbe.gatech.edu

1. K. A. Janes, J. G. Albeck, S. Gaudet, P. K. Sorger, D. A. Lauffenburger and M. B. Yaffe, *Science*, 2005, **310**, 1646-1653.
2. T. Reya and H. Clevers, *Nature*, 2005, **434**, 843-850.
3. C. Sander, *Science*, 2000, **287**, 1977-1978.
4. J. B. Gibbs, *Science*, 2000, **287**, 1969-1973.
5. S. Gaudet, K. A. Janes, J. G. Albeck, E. A. Pace, D. A. Lauffenburger and P. K. Sorger, *Mol Cell Proteomics*, 2005, **4**, 1569-1590.
6. B. Schoeberl, C. Eichler-Jonsson, E. D. Gilles and G. Muller, *Nat Biotechnol*, 2002, **20**, 370-375.
7. M. L. Kemp, L. Wille, C. L. Lewis, L. B. Nicholson and D. A. Lauffenburger, *Journal of Immunology*, 2007, **178**, 4984-4992.
8. H. E. Kohrt, C. T. Shu, T. B. Stuge, S. P. Holmes, J. Weber and P. P. Lee, *J Immunother (1997)*, 2005, **28**, 297-305.
9. B. N. Kholodenko, O. V. Demin, G. Moehren and J. B. Hoek, *Journal of Biological Chemistry*, 1999, **274**, 30169-30181.
10. R. N. Germain and I. Stefanova, *Annu Rev Immunol*, 1999, **17**, 467-522.
11. K. Sachs, O. Perez, D. Pe'er, D. A. Lauffenburger and G. P. Nolan, *Science*, 2005, **308**, 523-529.
12. J. El-Ali, P. K. Sorger and K. F. Jensen, *Nature*, 2006, **442**, 403-411.
13. A. Groisman, C. Lobo, H. J. Cho, J. K. Campbell, Y. S. Dufour, A. M. Stevens and A. Levchenko, *Nature Methods*, 2005, **2**, 685-689.
14. S. Paliwal, P. A. Iglesias, K. Campbell, Z. Hilioti, A. Groisman and A. Levchenko, *Nature*, 2007, **446**, 46-51.
15. K. R. King, S. Wang, A. Jayaraman, M. L. Yarmush and M. Toner, *Lab on a Chip*, 2008, **8**, 107-116.
16. J. El-Ali, S. Gaudet, A. Gunther, P. K. Sorger and K. F. Jensen, *Analytical Chemistry*, 2005, **77**, 3629-3636.
17. H. Lu, M. A. Schmidt and K. F. Jensen, *Lab On A Chip*, 2005, **5**, 23-29.
18. M. A. McClain, C. T. Culbertson, S. C. Jacobson, N. L. Allbritton, C. E. Sims and J. M. Ramsey, *Anal. Chem*, 2003, **75**, 5646–5655.
19. C. E. Sims and N. L. Allbritton, *Lab on a Chip*, 2007, **7**, 423-440.
20. P. J. Lee, P. J. Hung, V. M. Rao and L. P. Lee, *Biotechnol. Bioeng*, 2006, **94**, 5–14.
21. D. D. Carlo, C. Ionescu-Zanetti, Y. Zhang, P. Hung and L. P. Lee, *Lab on a Chip*, 2005, **5**, 171-178.
22. A. E. Herr, A. V. Hatch, D. J. Throckmorton, H. M. Tran, J. S. Brennan, W. V. Giannobile and A. K. Singh, *Proceedings of the National Academy of Sciences*, 2007, **104**, 5268.
23. A. P. Sudarsan and V. M. Ugaz, *Proceedings of the National Academy of Sciences*, 2006, **103**, 7228-7233.
24. A. D. Stroock, S. K. W. Dertinger, A. Ajdari, I. Mezic, H. A. Stone and G. M. Whitesides, *Science*, 2002, **295**, 647-651.
25. P. B. Howell, D. R. Mott, S. Fertig, C. R. Kaplan, J. P. Golden, E. S. Oran and F. S. Ligler, *Lab on a Chip*, 2005, **5**, 524-530.
26. J. T. Yang, K. J. Huang and Y. C. Lin, *Lab on a Chip*, 2005, **5**, 1140-1147.
27. D. R. Mott, P. B. Howell, J. P. Golden, C. R. Kaplan, F. S. Ligler and E. S. Oran, *Lab on a Chip*, 2006, **6**, 540-549.
28. F. M. White, McGraw-Hill Publishers: New York, 1999.
29. Y. N. Xia and G. M. Whitesides, *Annual Review of Materials Science*, 1998, **28**, 153-184.
30. M. Migliori, D. Gabriele, R. Di Sanzo, B. de Cindio and S. Correra, *Journal of Chemical and Engineering Data*, 2007, **52**, 1347-1353.
31. W. M. Deen, *Analysis of Transport Phenomena* Oxford University Press, Inc., New York, New York, 1998.

32. L. T. Lam, R. E. Davis, J. Pierce, M. Hepperle, Y. Xu, M. Hottelet, Y. Nong, D. Wen, J. Adams, L. Dang and L. M. Staudt, *Clinical Cancer Research*, 2005, **11**, 28-40.
33. S. P. Wu, S. Ringgaard, S. Oyre, M. S. Hansen, S. Rasmus and E. M. Pedersen, *Journal of Magnetic Resonance Imaging*, 2004, **19**, 188-193.
34. J. E. Kim and F. M. White, *J Immunol*, 2006, **176**, 2833-2843.
35. I. H. Khan, S. Mendoza, P. Rhyne, M. Ziman, J. Tuscano, D. Eisinger, H. J. Kung and P. A. Luciw, *Mol Cell Proteomics*, 2006, **5**, 758-768.

REFERENCES

Abbas A. K., Autoimmunity Reviews 2, 2003, 115–118.

Barber, L. D., S. Jordan, et al, J Immunol Methods, 2006, 314(1-2):147-52.

Beebe, D. J., J. S. Moore, et al, Nature, 2000, 404(6778): 588.

Beebe DJ, Mensing GA, Walker GM, Annual Review or Biomedical Engineering, 2002, 4, 261-286

Carlo D. D., Ionescu-Zanetti C., Zhang Y., Hung P. and Lee L. P.,Lab on a Chip, 2005, 5, 171-178.

Chiu, D. T., N. L. Jeon, et al, Proceedings Of The National Academy Of Sciences Of The United States Of America, 2000, 97(6): 2408-2413.

Chung, B. G., L. A. Flanagan, et al, Lab On A Chip, 2005, 5(4): 401-406.

Dang, Y., K. L. Knutson, et al, Clin Cancer Res, 2007, 13(6): 1883-91.

Deen W. M., Analysis of Transport Phenomena Oxford UniversityPress, Inc., New York, New York, 1998.

DeSilva, D. R., E. A. Jones, et al, Cell Immunol, 1997, 180(2): 116-23.

Dudley M. E., Wunderlich J. R., Robbins P. F., Yang J. C., Hwu P., Schwartzentruber D. J., Topalian S. L., Sherry R., Restifo N. P., Hubicki A. M., Robinson M. R., Raffeld M., Duray P., Seipp C. A., Rogers-Freezer L., Morton K. E., Mavroukakis S. A., White D. E. and Rosenberg S. A., Science, 2002, 298, 850-854.

Duffy, D. C., J. C. McDonald, et al, Anal. Chem., 1998, 70: 4974-4984.

El-Ali J., Gaudet S., Gunther A., Sorger P. K. and Jensen K. F., Analytical Chemistry, 2005, 77, 3629-3636.

El-Ali J., Sorger P. K. and Jensen K. F., Nature, 2006, 442, 403-411.

Gaudet S., Janes K. A., Albeck J. G., Pace E. A., Lauffenburger D. A.. and Sorger P. K., Mol Cell Proteomics, 2005, 4, 1569-1590.

Germain R. N. and Stefanova I., Annu Rev Immunol, 1999, 17, 467-522.

Gibbs J. B., Science, 2000, 287, 1969-1973.

Groisman A., Lobo C., Cho H. J., Campbell J. K., Dufour Y. S., Stevens A.M. and Levchenko A., Nature Methods, 2005, 2, 685-689.

Han, J. and H. G. Craighead, Science, 2000, 288(5468): 1026-1029.

Heisel, O. and P. Keown, Transplantation, 2001, 72(8): 1416-22.

Herr A. E., Hatch A. V., Throckmorton D. J., Tran H. M., Brennan J. S., Giannobile W. V. and Singh A. K., Proceedings of the National Academy of Sciences, 2007, 104, 5268.

Ho, W. Y., H. N. Nguyen, et al, J Immunol Methods, 2006, 310(1-2): 40-52.

Howe, C. J., M. M. LaHair, et al, Assay Drug Dev Technol, 2003, 1(4): 537-44.

Howell Jr, P. B., D. R. Mott, et al, Lab Chip, 2005, 5: 524-530.

Howell P. B., Mott D. R., Fertig S., Kaplan C. R., Golden J. P., Oran E. S. and Ligler F. S., Lab on a Chip, 2005, 5, 524-530.

Huang, L. R., E. C. Cox, et al, Science, 2004, 304(5673): 987-990.

Irimia, D., Tompkins, R. G., Toner, M., Anal. Chem. 2004, 76, 6137–6143.

Janes K. A. , Albeck J. G., Gaudet S., Sorger P. K., Lauffenburger D. A. and Yaffe M. B., Science, 2005, 310, 1646-1643.

Janes, K. A., J. G. Albeck, et al, Mol Cell Proteomics, 2003, 2(7): 463-73.

Jerome K. R., Journal of virology, 2008, 82: 9, 4194-204.

June C. H., J Clin Invest, 2007, 117, 1466-1476.

Kalamasz, D., S. A. Long, et al J Immunother, 2004, 27(5): 405-18.

Kemp M. L., Wille L., Lewis C. L., Nicholson L. B. and Lauffenburger D. A., Journal of Immunology, 2007, 178, 4984-4992.

Kenis, P. J. A., R. F. Ismagilov, et al. Science, 1999, 285(5424): 83-85.

Khan I. H., Mendoza S., Rhyne P., Ziman M., Tuscano J., Eisinger D., Kung H. J. and Luciw P. A., Mol Cell Proteomics, 2006, 5, 758-768.

Kholodenko B. N., Demin O. V., Moehren G. and Hoek J. B., Journal of Biological Chemistry, 1999, 274, 30169-30181.

Kim J. E. and White F. M., J Immunol, 2006, 176, 2833-2843.

Kim J., Jang S. H., Jia G., Zoval J.V., Da Silva N. A. and Madou M.J., Lab Chip, 2004, 4, 516 – 522.

King K. R., Wang S., Jayaraman A., Yarmush M.L. and Toner M.,Lab on a Chip, 2008, 8, 107-116.

Kohrt H. E., Shu C. T., Stuge T. B., Holmes S. P., Weber J. and Lee P. P., J Immunother (1997), 2005, 28, 297-305.

Kosar, T. F., A. Tourovskaia, et al, Lab On A Chip, 2006, 6(5): 632-638.

Lam L. T., Davis R. E., Pierce J., Hepperle M., Xu Y., Hottelet M., Nong Y., Wen D., Adams J., Dang L. and Staudt L. M., Clinical Cancer Research, 2005, 11, 28-40.

Lee P. J., Hung P. J., Rao V. M. and Lee L. P., Biotechnol. Bioeng, 2006, 94, 5–14.

Lee, C. C., G. D. Sui, et al, Science, 2005, 310(5755): 1793-1796.

Lee, J. N., C. Park, et al, Anal. Chem, 2003, 75(23): 6544-6554.

Lu H., Schmidt M. A. and Jensen K. F., Lab On A Chip, 2005, 5, 23-29.

Lu, H., L. Y. Koo, et al, Analytical Chemistry, 2004, 76(18): 5257-5264.

Lu, H., M. A. Schmidt, et al, Lab On A Chip ; 2005, 5(1): 23-29.

Lu, H., S. Gaudet, et al, Analytical Chemistry, 2004, 76(19): 5705-5712.

Lucchetta, E. M., J. H. Lee, et al, Nature, 2005, 434(7037): 1134-1138.

Matter, M., V. Pavelic, et al, Cancer Res, 2007, 67(15): 7467-76.

Maus, M. V., A. K. Thomas, et al, Nat Biotechnol, 2002, 20(2): 143-8.

Maus, M. V., J. L. Riley, et al, Clin Immunol, 2003, 106(1): 16-22.

Mazzatti, D. J., G. Pawelec, et al, Proteome Sci, 2007, 5: 7.

Mazzatti D. J., White A., Forsey R. J., Powell J. R., and Pawelec G., Aging Cell. 2007 April 1; 6(2): 155–163.

McClain M. A., Culbertson C. T., Jacobson S. C., Allbritton N. L., Sims C.E. and Ramsey J. M., Anal. Chem, 2003, 75, 5646–5655.

Migliori M., Gabriele D., Di Sanzo R., de Cindio B. and Correra S.,Journal of Chemical and Engineering Data, 2007, 52, 1347-1353.

Millet, L. J., M. E. Stewart, et al, Lab Chip, 2007, 7: 987-994.

Morgan, R. A., M. E. Dudley, et al, Science, 2006, 314(5796): 126-129.

Mott D. R., Howell P. B., Golden J. P., Kaplan C. R., Ligler F. S. and Oran E. S., Lab on a Chip, 2006, 6, 540-549.

Oelke, M., M. V. Maus, et al, Nat Med, 2003, 9(5): 619-24.

Ossendorp, F., E. Mengede, et al, The Journal of Experimental Medicine, 1998, 187(5): 93-702.

Paliwal S., Iglesias P. A., Campbell K., Hilioti Z., Groisman A. and Levchenko A., Nature, 2007, 446, 46-51.

Pawelec, G., M. Adibzadeh, et al, Vaccine, 2000, 18(16): 1666-74.

Peggs K. S., Quezada S. A., Allison J. P., Immunological Reviews 2008, Vol. 224: 141–165

Ravula, S. K., M. A. McClain, et al, Lab Chip, 2006, 6: 1530-1536.

Reya T and Clevers H, Nature, 2005, 434, 843-850

Riddell, S. R. and P. D. Greenberg, J Immunol Methods, 1990, 128(2): 189-201.

Sachs K., Perez O., Pe'er D., Lauffenburger D. A. and Nolan G. P., Science, 2005, 308, 523-529.

Salvador et all, Nat. Immunol., 2005, 6:390–395.124

Sander C., Science, 2000, 287, 1977-1978

Schoeberl B., Eichler-Jonsson C., Gilles E. D. and Muller G., Nat Biotechnol, 2002, 20, 370-375

Sims C. E. and Allbritton N. L., Lab on a Chip, 2007, 7, 423-440.

Song J. et al, Cellular & Molecular Immunology, 2008, 5(4):239-247.

Staveley-O'Carroll, K., E. Sotomayor, et al, Proceedings of the National Academy of Sciences, 1998, 95(3): 1178-1183.

Stroock A. D., Dertinger S. K. W., Ajdari A., Mezic I., Stone H. A. and Whitesides G. M., Science, 2002, 295, 647-651.

Stroock, A. D. and G. J. McGraw, Sciences, 2000, 362(1818): 971-986.

Sudarsan A. P. and Ugaz V. M., Proceedings of the National Academy of Sciences, 2006, 103, 7228-7233.

Takayama, S., E. Ostuni, et al, Nature, 2001, 411(6841): 1016-1016.

Tan, Y. C., J. S. Fisher, et al, Lab On A Chip, 2004, 4(4): 292-298.

Thompson, J. A., R. A. Figlin, et al, Clin Cancer Res, 2003, 9: 3562-70.

Thorsen, T., S. J. Maerkl, et al, Science, 2002, 298(5593): 580-584.

Utada, A. S., E. Lorenceau, et al, Science, 2005, 308(5721): 537-541.

Wang, H. Y., Lu, C., Anal. Chem. 2006, 78, 5158–5164.

Whitesides, G. M., Nature, 2006, 442(7101): 368-373.

Wu S. P., Ringgaard S., Oyre S., Hansen M. S., Rasmus S. and Pedersen E. M., Journal of Magnetic Resonance Imaging, 2004, 19, 188-193.

Wu, H. K., Wheeler, A., Zare, R. N., Proc. Natl. Acad. Sci. USA, 2004, **101**, 12809-12813.

Xia Y. N. and Whitesides G. M., Annual Review of Materials Science, 1998, 28, 153-184.

Yang J. T., Huang K. J. and Lin Y. C., Lab on a Chip, 2005, 5, 1140-1147.

Yee, C., J. A. Thompson, et al,The Journal of Experimental Medicine, 2000, 192(11): 1637-1644.

Zippelius, A., P. Batard, et al, Cancer Research, 2004, 64(8): 2865-2873.

Zou, W., Nat Rev Cancer, 2004, 5(4): 263-74.